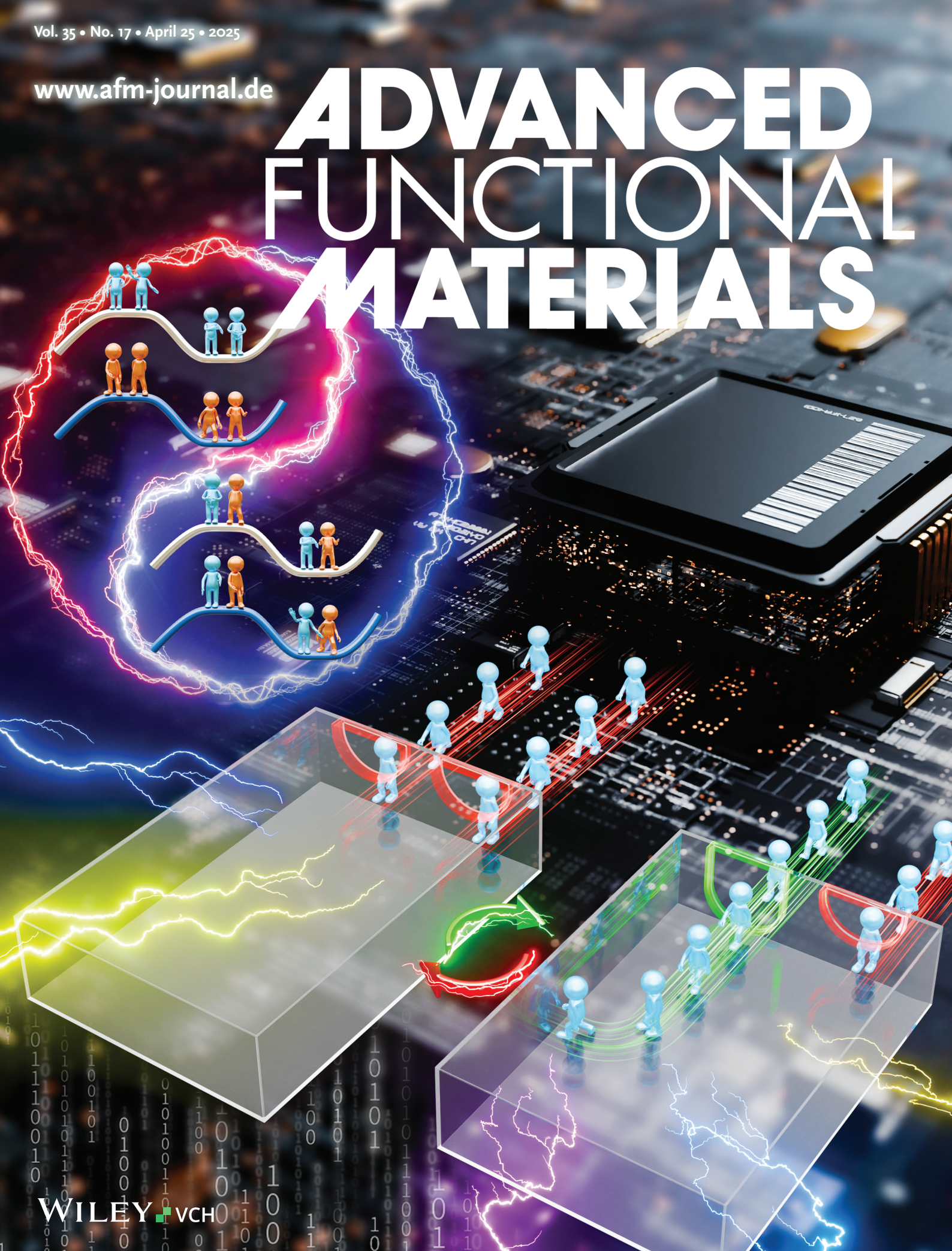
Vol. 35 • No. 17 • April 25 • 2025

www.afm-journal.de

ADVANCED FUNCTIONAL MATERIALS



WILEY VCH

Ultrafast level sensitivity and cutting edge elemental analysis in semiconductor manufacturing
Discover now

ADVANCED FUNCTIONAL MATERIALS

Advanced Functional Materials: Volume 35, Issue 17

April 25, 2025

‹ Previous Issue | Next Issue ›

GO TO SECTION

Export Citation(s) Download PDF(s)

Cover Picture

Free Access

Electric-Field- and Stacking-Tuned Antiferromagnetic FeClF Bilayer: The Coexistence of Bipolar Magnetic Semiconductor and Anomalous Valley Hall Effect (Adv. Funct. Mater. 17/2025)

Long Zhang, Yuqi Liu, Menghao Wu, Guoying Gao

First Published: 25 April 2025



Ferrovalley
In article number 2417857, Guoying Gao and co-workers present the reversible electric field switch in bilayer FeClF for the appearance and disappearance of anomalous valley Hall effect in the cubsids, and the transition of bipolar magnetic semiconductor and antiferromagnetic semiconductor in the Tai Chi diagram, indicating the promising encoding, transport and storage of information through valley and spin.

Abstract | PDF | Request permissions

Inside Front Cover

Free Access

Manipulation of the Electronic Structure of Ruthenium Nanoclusters by Ni-N_4 Sites Enhances the Alkaline Hydrogen Evolution Reaction (Adv. Funct. Mater. 17/2025)

Qingiong Zhang, Mengmeng Lao, Yuanyuan Yu, Xinzhi Ma, Moyan Li, Zhaofu Fei, Paul J. Dyson, Shuanghe Wang, Douyong Min

First Published: 25 April 2025



Ruthenium Nanoclusters
In article number 2416271, Zhaofu Fei, Paul J. Dyson, Douyong Min, and co-workers develop a highly active electrocatalyst for alkaline hydrogen evolution by precisely tuning the electronic structure of Ru nanoclusters via an atomic Ni-N_4 containing support. The electrocatalyst exhibits remarkable stability for over 1000 hours and exceeding the benchmarks required for industrial hydrogen production.

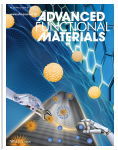
Inside Back Cover

Free Access

High-Crystallinity Wrinkled Hard Carbon via Molecular-Level Anchoring Glucose Molecules with Cooperative-Assembly of Intermolecular Hydrogen Bonds for Sodium-Ion Batteries (Adv. Funct. Mater. 17/2025)

Yanni Wang, Wenwen Li, Chengxiang Huang, Zhou Jiang, Fuxi Liu, Xinyan Zhou, Wei Zhang, Weitao Zheng

First Published: 25 April 2025



Intermolecular Hydrogen Bonds
In article number 2420580, Wei Zhang and co-workers establish an innovative strategy for synthesizing hard carbon materials with high crystallinity and highly-exposed surfaces by leveraging the anchoring effect of molecularly bonded hydrogen bonds in carbon precursor molecules. This approach allows for precise control of intermolecular forces and thereby enables highly predictable synthesis of innovative materials.

Abstract | PDF | Request permissions

Back Cover

Free Access

Versatile Foldable Inkjet-Printed Thermoacoustic Loudspeaker on Paper (Adv. Funct. Mater. 17/2025)

Hyungyu Im, Eunhwan Jo, Yunsung Kang, Jongbaeg Kim

First Published: 25 April 2025



Flexible Electronics
In article number 2415218, Yunsung Kang, Jongbaeg Kim, and co-workers present the innovative concept of inkjet-printed thermoacoustic loudspeakers on paper, utilizing carbon nanotubes to produce sound through heat. This combination enables versatile applications, turning ordinary paper into audio-emitting surfaces. In the cover image, the scene demonstrates how this technology can be applied in various forms, ranging from simple designs to complex origami structures.

Abstract | PDF | Request permissions

Issue Information

Free Access

Issue Information

First Published: 25 April 2025

PDF | Request permissions

Correction

Review

Open Access

Recent Advances in Highly Luminescent Carbon Dots

Yupeng Liu, Zhujun Huang, Xuanye Wang, Yiming Hao, Junxiang Yang, Hui Wang, Songsan Qu

First Published: 23 December 2024



Here, a comprehensive summary of the advancements is provided in highly luminescent carbon dots across various luminescence bands since their discovery in 2004. It systematically covers the synthesis, structural characteristics, preparation strategies, and essential purification of these carbon dots, along with their applications in efficient luminescence. Finally, the current challenges are discussed and insights into future developments are offered.

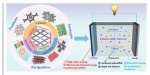
Abstract | Full text | PDF | References | Request permissions

Full Access

Covalent Organic Frameworks and Their Derivatives for Applications in High-Performance Lithium–Sulfur Batteries

Xiudong Chen, Huixiang Jiang, Jin-Hang Liu, Hang Zhang, Changchao Zhan, Yun Gao, Xiaodou Jiang, Yawei Wang, Xiaohua Cao, Shu-Lei Chou

First Published: 30 December 2024



This review summarizes the latest progress and challenges in the application of COFs and their derivatives in lithium-sulfur batteries (LSBs), systematically analyzes the application of COFs-based materials as sulfur cathode host materials, modified separators, and electrolytes, focuses on the impact of the structure and optimization strategy of COF-based materials on the performance of LSBs, and provides prospects for the future development of COF-based materials with better energy storage performance.

Abstract | Full text | PDF | References | Request permissions

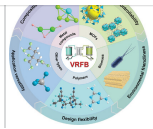
Full Access

Precursor Engineering for the Electrode of Vanadium Redox Flow Batteries

Shangkun Wang, Yingqiao Jiang, Zemin Feng, Yongguang Liu, Long Jiang, Lei Dai, Jing Zhu, Ling Wang, Zhangqing He

First Published: 29 December 2024

This review provides an in-depth analysis of precursor engineering for the electrodes of vanadium redox flow batteries (VRFBs), which describe characterization and processing techniques for various types of precursors. Precursor engineering for electrode modulation and performance optimization is further discussed. The review also provides a prospective study on precursor engineering development and the development of VRFBs.



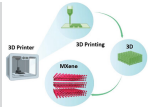
Abstract | Full text | PDF | References | Request permissions

Open Access

MXene 3D/4D Printing: Ink Formulation and Electrochemical Energy Storage Applications

Shaista Nousheen, Martin Pumera

First Published: 17 February 2025



A comprehensive study of MXene printing technique is presented, focusing on MXene ink formulation, surface chemistry, rheological characteristics, physical storage, and ink stability. Different printing techniques, such as 3D/4D printing, screen printing, inkjet printing, and continuous liquid interface production printing along with their applications in electrochemical energy storage, specifically in supercapacitors and batteries, are discussed.

Abstract | Full text | PDF | References | Request permissions

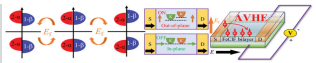
Research Article

Full Access

Electric-Field- and Stacking-Tuned Antiferromagnetic FeClF Bilayer: The Coexistence of Bipolar Magnetic Semiconductor and Anomalous Valley Hall Effect

Long Zhang, Yuqi Liu, Menghao Wu, Guoying Gao

First Published: 14 November 2024



The reversible electric-field and stacking effect on valley- and spin-polarized electrons of AFM Janus FeClF bilayer is investigated to probe the interplay of spin, valley and layer degrees of freedom. Spontaneous PMA, concurrent and controllable BMS and AVHE by reversible electric-field suggest the promising design of ferrovalley BMSs and application of multifunctional valleytronics and spintronics for 2D Janus ferrum dichlorides.

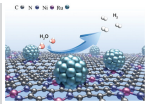
Abstract | Full text | PDF | References | Request permissions

Full Access

Manipulation of the Electronic Structure of Ruthenium Nanoclusters by Ni-N_4 Sites Enhances the Alkaline Hydrogen Evolution Reaction

Qingiong Zhang, Mengmeng Lao, Yuanyuan Yu, Xinzhi Ma, Moyan Li, Zhaofu Fei, Paul J. Dyson, Shuanghe Wang, Douyong Min

First Published: 01 December 2024



A catalyst comprising ruthenium nanoclusters immobilized on a carbon substrate containing single-atom Ni-N_4 sites is synthesized and evaluated in the alkaline hydrogen evolution reaction. The electronic properties of the ruthenium nanoclusters effectively lower the water dissociation barrier, thus achieving high efficiency and stability in hydrogen production.

Abstract | Full text | PDF | References | Request permissions

Xiangliang Sun, Chunlei Zhang, Danpeng Gao, Shoufeng Zhang, Bo Li, Jianqiu Gong, Shuai Li, Shuang Xiao, Zongliang Zhu, Zhongran Li

First Published: 20 December 2024

This article corrects the following:

Boosting Efficiency and Stability of NiO_x-Based Inverted Perovskite Solar Cells Through D-A Type Semiconductor Interface Modulation

Xiangliang Sun, Chunlei Zhang, Danpeng Gao, Shoufeng Zhang, Bo Li, Jianqiu Gong, Shuai Li, Shuang Xiao, Zongliang Zhu, Zhongran Li

Volume 34, Issue 25, Advanced Functional Materials | First Published online: January 9, 2024

Full text | PDF | Request permissions

Frontispiece

Free Access

Long, Fibrous, and Tailorable Dielectric Elastomer Artificial Muscles via Mask-Free Stamping of Carbon Nanotube Electrodes (Adv. Funct. Mater. 17/2025)

Qi Shao, Liang Zhou, Jingjo Zhou, Xin-Jun Liu, Huichan Zhao

First Published: 25 April 2025



Artificial Muscles
This cover illustrates the potential of dielectric elastomer (DE) artificial muscles in robotics. The main image features a DE-driven robotic arm, revealing the microscopic structure of rolled DE artificial muscles with interleaved flexible electrodes and elastic dielectrics. The background showcases a blurred array of robots, highlighting the broad applications of this technology. More information can be found in article number 2422905 by Huichan Zhao and co-workers.

Abstract | PDF | Request permissions

Research Article

Full Access

Long, Fibrous, and Tailorable Dielectric Elastomer Artificial Muscles via Mask-Free Stamping of Carbon Nanotube Electrodes

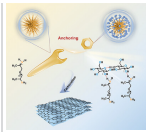
Qi Shao, Liang Zhou, Jingjo Zhou, Xin-Jun Liu, Huichan Zhao

First Published: 13 January 2025

A comprehensive approach for fabricating and actuating long fibrous dielectric elastomer artificial muscles is presented. The method features mask-free patterning of large-area carbon nanotube electrodes, an amplitude modulation algorithm for high-frequency actuation, and integration of a stretchable waveguide sensor. The resulting 180-mm artificial muscles demonstrate human muscle-like performance and can be segmented into shorter units for various robotic applications.

Yanni Wang, Wenwen Li, Chengxiang Huang, Zhou Jiang, Fuxi Liu, Xinyan Zhou, Wei Zhang, Weitao Zheng

First Published: 15 December 2024



An innovative strategy for synthesizing hard carbon materials with high crystallinity and highly-exposed surfaces is established by leveraging the anchoring effect of molecularly bonded hydrogen bonds in carbon precursor molecules. This approach allows for precise control of intermolecular forces and thereby enables highly predictable synthesis of innovative materials.

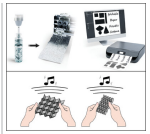
Abstract | Full text | PDF | References | Request permissions

Full Access

Versatile Foldable Inkjet-Printed Thermoacoustic Loudspeaker on Paper

Hyungyu Im, Eunhwan Jo, Yunsung Kang, Jongbaeg Kim

First Published: 24 November 2024



This study presents a thin and flexible loudspeaker with scalable fabrication, offering new sound applications such as foldability, stretchability, and omnidirectional sound emission. Utilizing inkjet-printed CNT-based inks on paper, the loudspeakers achieve high sound pressure levels and exceptional mechanical durability, even under significant deformation. These properties enable innovative audio applications demonstrating the potential for versatile, space-efficient audio solutions.

Abstract | Full text | PDF | References | Request permissions

Frontispiece

Free Access

Hot-Injection Synthesis of Metal Organochalcogenide Nanocrystals with Tunable Compositions and Competitive Hole Mobility (Adv. Funct. Mater. 17/2025)

Pimpan Leangtanom, Ratsapon Khamlue, Achawee Dangkongkla, Petcharaphorn Chatsiri, Watcharaphol Paritmongkol

First Published: 25 April 2025



Metal Organochalcogenide Nanocrystals
In article number 2423516, Watcharaphol Paritmongkol and co-workers report the first hot-injection synthesis of AgGePh nanocrystals, a metal organochalcogenide (MOC) semiconductor. This method enables precise size control, extends to various chalcogen compositions, and ensures colloidal stability for over 4 weeks. With high thermal stability and p-type transport, AgGePh exhibits high hole mobility and holds promise for thin-film optoelectronic applications.

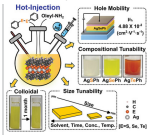
Abstract | PDF | Request permissions

Full Access

Hot-Injection Synthesis of Metal Organochalcogenide Nanocrystals with Tunable Compositions and Competitive Hole Mobility

Pimpan Leangtanom, Ratsapon Khamlue, Achawee Dangkongkla, Petcharaphorn Chatsiri, Watcharaphol Paritmongkol

First Published: 18 February 2025



A high-yield hot-injection synthesis produces high-quality AgGePh nanocrystals within 15 s, maintaining colloidal stability and crystallinity for device integration. The process enables size control and extends to other MOCs for tunable optical properties. AgGePh exhibits thermal stability, p-type behavior, and high hole mobility, making it a competitive candidate for optoelectronic applications.

Abstract | Full text | PDF | References | Request permissions



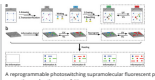
Abstract | Full text | PDF | References | Request permissions

Full Access

Reprogrammable Supramolecular Fluorescent Polymers for Rewritable Information Encryption and Anti-Counterfeiting

Yong Tian, Baoyu Huang, Shun He, Yi Zhao, Kairong Zang, Hong Wang, Xiaomei Zhao, Jiaxi Cui, Jian Chen

First Published: 15 December 2024



A reprogrammable photoswitching supramolecular fluorescent polymer (FSFP) is prepared based on self-growing methods and host–guest interactions, which can be used for rewritable information encryption and anti-counterfeiting.

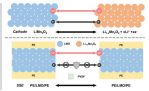
Abstract | Full text | PDF | References | Request permissions

Full Access

Another Way to Realize $LiMn_2O_4$ as a Solid Electrolyte

Jingzhen Du, Zewen Sun, Bohao Peng, Xuming Xu, Lijun Fu, Yuhui Chen, Lili Liu, Xu Liu, Yuping Wu

First Published: 19 December 2024



The electronic conductivity of the commercial active cathode material $LiMn_2O_4$ is sharply reduced, and then a low-cost, environmentally friendly, and high-performance solid-state electrolyte based on $LiMnO_2$ is achieved with excellent electrochemical performance.

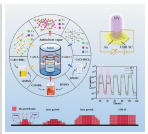
Abstract | Full text | PDF | References | Request permissions

Full Access

Halide Tunable Perovskite Single Crystals as Efficient Photodetector

Sancan Han, Shan Zhu, Guohao Fan, Xingcan Huang, Guangyao Zhao, Rui Shi, Ya-Huang, Mengge Wu, Jian Li, Yuan Guo, Yuyu Gao, Songlin Zhuang, Fa Cao, Xinge Yu, Dawei Zhang

First Published: 20 December 2024



In this study, centimeter-sized $Cs_2Bi_2X_9$ (=I/Br/Cl) single crystals are first synthesized during a 2-day control period, leveraging a synergistic nucleation and supersaturation engineering approach in a low-temperature solution of ≈ 50 °C, which provides unprecedented advantages, including effortless tunability of various X elements and a notably accelerated growth time, achieving the application in photoimaging and optical communication compiled with Morse code.

Abstract | Full text | PDF | References | Request permissions

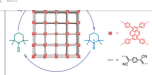
Full Access

Local Charge Regulation in Selenides via High-Entropy Engineering to Boost Electromagnetic Wave Absorption

Zhikai Yan, Lei Wang, Yiqian Du, Guanyu Chen, Yuyang Wu, Liting Yang, Wentin You, Biao Zhao, Renchao Che

First Published: 17 December 2024

Abstract | Full text | PDF | References | Request permissions



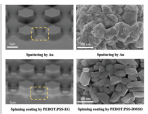
Abstract | Full text | PDF | References | Request permissions

Full Access

Topographic Scanning Electronic Microscopy Reveals the 3D Surface Structure of Materials

Wen Sun, Yichen Xu, Ying Zhou, Zhihan Zang, Lei Wang, Jianyong Ouyang

First Published: 19 December 2024



A thin PEDOT:PSS film is used to replace Au thin film as the conductive layer for SEM characterization. The SEM images can provide detailed information on not only the horizontal but also the vertical structure of the surface and exhibit high resolution. They can detect underlying structures and nanostructured surfaces. This technology is called the topographic SEM.

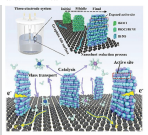
Abstract | Full text | PDF | References | Request permissions

Full Access

Unlocking Interfacial Dynamics of Porous Electrode via Vertical-Aligned Bismuth-Nanosheet Decorating for Vanadium Redox Flow Batteries

Zihan Yu, Xiongjie Jia, Huan Gao, Ruihang Su, Xiaoyi Wang, Tianshou Zhao, Haoran Jiang

First Published: 19 December 2024



To achieve a coupled enhancement of catalytic and transport properties, and further unlock interfacial dynamics of the electrode, vertical-aligned bismuth-nanosheets are in situ decorated on the surface of the porous electrode in this paper. This advanced method can greatly release the performance of the electrode, improve battery performance, and enhance the application potential of vanadium redox flow batteries.

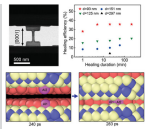
Abstract | Full text | PDF | References | Request permissions

Full Access

Highly Efficient Self-Healing of Fractured Ti_3AlC_2 MAX Phase Nanowires

Junfeng Cui, Xiaobi Hu, Lei Zhang, Xingying Yang, Youbing Li, Guoxin Chen, Chun Tang, Peiling Ke

First Published: 20 December 2024



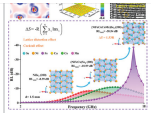
Intrinsic highly efficient self-healing phenomenon in Ti_3AlC_2 MAX phase nanowires at room temperature is reported. The self-healing efficiency of 36.2% is achieved on the fractured Ti_3AlC_2 nanowire after self-healing for 5 min, and the smaller the diameter, the higher the self-healing efficiency. The underlying mechanisms are uncovered by atomic-resolution characterizations combined with atomic simulations.

Abstract | Full text | PDF | References | Request permissions

Full Access

Efficient Separation of Adjacent Rare Earths in One Step by Using Ion-microporous Metal–Organic Frameworks

An-Min Song, Meng-jie Yang, Zhi Wu, Qing Yang, Bin Lin, Ru-Ping Liang, Jian-Ding Qiu



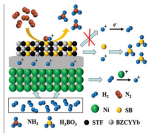
Abstract | Full text | PDF | References | Request permissions

Full Access

A Synergistic Hybrid of $Sr_2B_2O_5$ and $Sr_3Ti_{1.07}Fe_{0.93}O_{7-\delta}$ (γ < 1) as a Cathode for High-Performance Electrochemical Ammonia Synthesis via Protonic Ceramic Electrolysis Cells

Kaihui Wang, Wenyan Zan, Yawei Li, Si-Dian Li, Zongping Shao, Huidi Chen

First Published: 19 December 2024



This research develops a hybrid material consisting of $Sr_2B_2O_5$ and $Sr_3Ti_{1.07}Fe_{0.93}O_{7-\delta}$ (where γ<1) for the synthesis of ammonia through a protonic ceramic electrolysis cell. The incorporation of the proton acceptor $Sr_2B_2O_5$ is beneficial in suppressing the hydrogen evolution (HER) and enhancing the efficiency of the electrocatalytic nitrogen reduction reaction (eNRR).

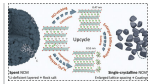
Abstract | Full text | PDF | References | Request permissions

Full Access

High Rate Performance of Single-Crystalline NCM Upcycled from Spent Lithium-Ion Batteries Via Direct Recovery and Modification

Kaipei Wang, Hao Zhang, Wentao Dou, Kunfang Wang, Tongyu Wang, Xin Su

First Published: 17 December 2024



A simple and effective upcycling method of single-crystalline NCM with surface modification from spent material is developed, significantly enhancing its rate performance at 10C and cycling stability ≈99% for 100 cycles.

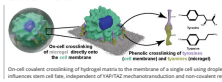
Abstract | Full text | PDF | References | Request permissions

Open Access

Covalent On-Cell Conjugation of Biomaterials Through Oxidative Phenolic Coupling Regulates Stem Cell Fate via Intracellular Biophysical Programming

Castro Johnbosco, Malin Becker, Niels Willemen, Marieke Meeling, Kannan Govindaraj, Tom Kamperman, Jeroen Leijten

First Published: 20 December 2024



On-cell covalent crosslinking of hydrogel matrix to the membrane of a single cell using droplet microfluidics enables mechanotransduction and influences stem cell fate. This newly established approach influences stem cell fate, independent of YAP/TAZ mechanotransduction and non-covalent reversible binding ligands yet by various intracellular biophysical programming at the cytoplasmic and nuclear level.

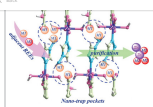
Abstract | Full text | PDF | References | Request permissions

Full Access

Unique H_2O Vortex in One New MOF Material Strengthening C_2H_6 Adsorption and Unprecedented Purification from $C_2H_2/C_2H_4/C_2H_6$ Mixtures

Lin Zhang, Rui-Cheng Gao, Xin Liu, Bin Zhang, Lei Hou, Yao-Yu Wang

First Published: 05 January 2025



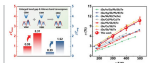
Abstract | Full text | PDF | References | Request permissions

Full Access

High Thermoelectric Performance and Energy Conversion in Hg-doped GeTe

Zhe Guo, Guangjie Wu, Minhui Yuan, Hongtao Li, Xiaojian Tan, Jianfeng Cai, Zongwei Zhang, Jing Shuai, Guoqiang Liu, Jun Jiang

First Published: 19 December 2024



The superior valence band convergence in in Hg-doped is revealed GeTe. Since the high is obtained and the κ_l is reduced, the thermoelectric performance of GeTe is significantly improved, leading to a greatly improved zT_{ave} of 1.52 between 300 and 773 K and a competitive conversion efficiency of 10.8% at ΔT = 530 K.

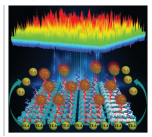
Abstract | Full text | PDF | References | Request permissions

Full Access

Ternary Heterojunction ZnS-ZnIn$_2$S$_4$-In$_2$S$_3$ Efficiently Catalyzes Triethylamine to Enhance Electrochemiluminescence Imaging Signals

Jingui Chen, Yue Jia, Huaiqing Zhao, Dan Wu, Yu Du, Xiang Ren, Qin Wei

First Published: 20 December 2024



Highly efficient catalysis: The ternary heterojunction semiconductor ZnS-ZnIn$_2$S$_4$-In$_2$S$_3$, vulcanized in situ by dual metal–organic frameworks, effectively catalyzes the swift production of free radicals from triethylamine through a step-by-step electron transfer process. This reaction leads to a notable enhancement in the luminescence of gold nanoclusters, ultimately resulting in an improved imaging resolution in electrochemiluminescence.

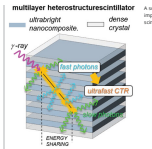
Abstract | Full text | PDF | References | Request permissions

Open Access

Highly Luminous Scintillating Nanocomposites Enable Ultrafast Time Coincidence Resolution for γ-rays Detection with Heterostructured Multilayer Scintillators

Matteo Salá, Matteo Orfano, Valeria Secchi, Ilaria Mattei, Nicolò Piama, Vojtech Zabloudil, Carsten Lowis, Romana Kučerková, Martin Nikl, Francesco Menardi, Blennette Auffray, Irene Villa, Angelo Monguzzi

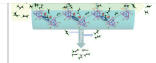
First Published: 19 December 2024



A scintillating polymeric composites loaded with hafnia nanoparticles is engineered to obtain a highly luminous material, thus achieving a 400% improvement of the scintillation yield under soft X-rays. The nanocomposite is employed to realize a multilayer heterostructured prototype scintillator than enable for ultrafast time coincidence resolution in the detection of 511 keV γ-rays used in ToF-PET.

Abstract | Full text | PDF | References | Request permissions

Full Access



A novel water-modified metal–organic framework (MOF) material with open hexagonal channels is reported, in which the unique water vortex formed in channels make the material have a significant preferential absorption effect on C_2H_6, resulting in the unprecedented one-step separation of $C_2H_6/C_2H_4/C_2H_2$ mixtures to give high-purity C_2H_6 and C_2H_2 products, respectively.

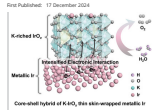
Abstract | Full text | PDF | References | Request permissions

Full Access

Alkali Metal-Induced Core-Shell Hybrid with Mixed Ir Valence State Boosts Acidic Water Oxidation

Liu Wang, Zijian Li, Haeseong Jang, Min Gyu Kim, Shanggyu Liu, Xuefeng Wang, Mengran Zeng, Jaephil Cho, Xien Liu, Qing Qin

First Published: 17 December 2024



Alkali metal K induced a core-shell hybrid of K-IrO_x thin skin-wrapped metallic Ir strengthens the electronic interaction and inhibits the overoxidation of Ir. Furthermore, the K enrichment in the IrO_x shell induces significant compressive stress, which tailors the properties of Ir−O bond not only stabilizing the lattice oxygen but also reducing the energy barrier of the rate-limiting step.

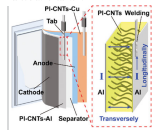
Abstract | Full text | PDF | References | Request permissions

Full Access

Ultralight Polymer-Based Current Collectors With Enhanced Transverse Conductivity via 3D Conductive Interlayers for Safe and High-Energy Lithium-Ion Batteries

Nuo Li, Jie Zhao, Yue Zhang, Ruifeng Song, Nan Zhang, Yanming Cui, Jia Lin, Henghui Xu, Yunhui Huang

First Published: 19 December 2024



The newly designed PBCCs are constructed by incorporating CNTs as fillers into the polymer PI with two metal layers coating, which exhibit lower mass density, enhance metal-polymer bonding force, and improve fracture strength. The obtained PBCCs not only guarantee longitudinal and transverse conductivity but also improve the battery's energy density and safety performance.

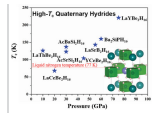
Abstract | Full text | PDF | References | Request permissions

Full Access

Design of High-T_c Quaternary Hydrides Under Moderate Pressures Through Substitutional Doping

Xudong Wei, Xiaokuan Hao, Xiaosu Song, Jingyu Niu, Guoying Gao, Yongjun Tian

First Published: 23 December 2024



A series of quaternary AA'_2H_{16} hydrides with a P4/nmm space group are constructed. Eight thermodynamically stable hydrides are selected and they are all potential superconductors, such as $LaTiBe_2H_{16}$ (126 K at 10 GPa), $YCaBe_2H_{16}$ (106 K at 45 GPa), $AcBeSiH_{16}$ (137 K at 30 GPa), $AcSr_2Si_2H_{16}$ (123 K at 30 GPa) and $LaYBe_2H_{16}$ (221 K at 75 GPa).

Abstract | Full text | PDF | References | Request permissions

Full Access

A 2D sp^2 Carbon Conjugated Pyrene Covalent Organic Framework with TEMPO for Selective Photocatalysis

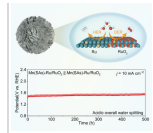
Huimin Hao, Fulin Zhang, Xiaoxiao Wang, Fengwei Huang, Shengli Chen, Xianjun Lang

First Published: 20 December 2024

Cooperative photocatalysis between a highly crystalline sp^2 carbon-conjugated covalent organic framework, Py-sp^2c-COF, with TEMPO is successfully established for selective aerobic oxidation of amines induced by green light. TEMPO (2 mol%) acts as an electron–proton transfer mediator to facilitate the formation of imines by Py-sp^2c-COF photocatalysis. Superoxide radical anion is essential for closing the

Abstract | Full text | PDF | References | Request permissions

First Published: 19 December 2024



This work reports a facile strategy to regulate the charge redistribution at Ru sites in Ru_2RuO_7 heterostructures via single-site Mn dopants to optimize the adsorption of OOH^* and H^* at Ru sites, significantly boosting electrochemical kinetics for acidic overall water-splitting.

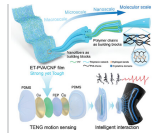
Abstract | Full text | PDF | References | Request permissions

Full Access

Multiscale Structural Strong yet Tough Triboelectric Materials Enabled by In Situ Microphase Separation

Peng Lu, Yang Yang, Bin Luo, Chenchen Cai, Tao Liu, Song Zhang, Mingchao Chi, Tong Zhao, Jinlong Wang, Xiangjiang Meng, Yayu Bai, Yuzheng Shao, Guoli Du, Shuangfei Wang, Shuangxi Nie

First Published: 23 December 2024



A strong yet tough triboelectric film is prepared via nanosilvent-induced polymer network reconfiguration, and a self-powered wearable motion sensor is integrated based on the film. The multiscale reinforced structures constructed by nanosilvent induce microphase separation strategy provide a novel solution for coordinating the conflicts between strength and toughness in heterogeneous polymer materials.

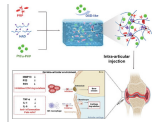
Abstract | Full text | PDF | References | Request permissions

Full Access

Nanozyme-Engineered Hyaluronic Acid Adhesives Loading Platelet-Rich Plasma for Multilayered Osteoarthritis Treatment with Pain-Relief Effect

Yiyang Zhao, Wanglin Duan, Bin Zhu, Yurong Chen, Ye Zhu, Sergio Martin-Saldaña, Zhengtao Xiao, Xinyi Liu, Luyao Feng, Yiming Ren, Yiting Gong, Fuquan Huo, Jinqing Li, Yuzhong Bu, Baoji Du, Liming Zhang

First Published: 23 December 2024



Here, the different enzyme-catalyzed activities of platinum–copper ($PtCu_3$) nanozymes are utilized at different pH values to directly catalyze the cross-linking of dopamine-modified hyaluronic acid (HAD), representing a new polymerization method for phenol-based bioadhesives. The resulting adhesive (HAD/$PtCu_3$/platelet-rich plasma (PRP)), when combined with PRP, significantly alleviates pain and improves the knee microenvironment in osteoarthritis rats, provides a promising alternative in osteoarthritis therapy.

Abstract | Full text | PDF | References | Request permissions

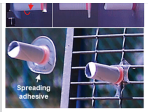
Full Access

Dynamically Spreading Shootable Adhesives Inspired by Dough Spinning

Sungbum Cho, Changeui Hong, Hyungwook Yoo, Yonghwa Ji, Seungchan Lee, Meonggyun Kim, Minsung Lee, Dongwuk Jung, Daegyun Jung, Dongyeon Kim, Jaewook Lee, Jongho Lee

First Published: 20 December 2024

This work introduces an innovative shootable adhesive technology that enables secure adhesion to remote, physically inaccessible surfaces by dynamically spreading into a thin, wide soft disk through spinning. This breakthrough opens up new capabilities for deploying various objects such as functional electronics or mechanical wires to remote surfaces for various applications including tracking, monitoring, searching and rescuing.



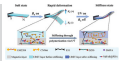
Abstract | Full text | PDF | References | Request permissions

Full Access

Heterogeneous Architecture Light-Responsive Stiffness-Tunable Magnetic Actuator

Chao Wu, Jiawei Li, Qiankun Zhang, Hongjun Kang, Zhimin Xie, Zhongjun Cheng, Qiang Tao, Dongjie Zhang, Yuyan Liu

First Published: 31 December 2024



Light-responsive tunable-stiffness material with bistable moduli is prepared by encapsulating double bonds in a polymer network. Next, the tunable-stiffness magnetic actuator is fabricated by introducing NdFeB@PDA and designed as a heterostructure. The actuator with fast deformation and stable state in both soft and stiffness is used in a variety of applications by cropping and magnetization.

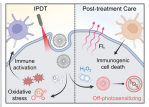
Abstract | Full text | PDF | References | Request permissions

Full Access

Off-Photosensitizing Derived Immuno-Photodynamic Therapy toward Postoperative Care

Jing Li, E Pang, Jusung An, Zhao Xiong, Eunji Kim, Minhuan Lan, Qian-Yong Cao, Jong Seung Kim

First Published: 29 December 2024



A novel H_2O_2-responsive photosensitizer, TBZPYBE, balances photodynamic therapy efficacy and postoperative safety. TBZPYBE self-quenches after ROS generation, converting to a non-toxic fluorescent derivative while releasing a glutathione scavenger to amplify therapy. Additionally, TBZPYBE promotes immune activation by enhancing dendritic cell maturation and macrophage polarization, offering a safer, immune-supportive approach to cancer therapy.

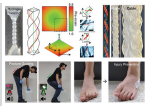
Abstract | Full text | PDF | References | Request permissions

Full Access

Hierarchical Tough Hydrogel with Enhanced Rigidity and Extensibility for Strain Sensing, Posture Guide, and Injury-Prevention

Nuri Park, Jiwan Fan, Jaeyun Kim

First Published: 23 December 2024



A method for modifying hydrogel structures through twisting is developed. This twisting creates helical and gradient polymer structures that enhance stress transfer, thereby improving the extensibility and toughness of the hydrogels. By assembling multiple hydrogel strands into higher hierarchies, beneficial mechanical properties are achieved. The advanced mechanical performance of these modified hydrogels supports successful applications in strain sensing, posture guidance, impact absorption, and injury prevention.

Abstract | Full text | PDF | References | Request permissions

Full Access

An Endothelium-Mimicking, Healable Hydrogel Shield for Bioprosthetic Heart Valve with Enhanced Intravascular Biocompatibility

Micharu Matsusong, Tunchen Ren, Ying Gao, Xiaojian Hong, Kaicheng Deng, Lin Yao, Si Cheng, Ruhao Zhou, Ying Lin, Gefei Tian, Jing Zhao, Peng Li, Xianbao Liu, Jianlan Wang

First Published: 15 January 2025

An endothelium-mimicking, healable hydrogel coating is introduced on porcine pericardium, aiming to address the limited service life of bioprosthetic heart valves (BHVs). The physically crosslinked polyvinyl alcohol hydrogel shield is repaired within 20 s under the photothermal effect of polydopamine nanoparticles; the conjugated selenocystamine enables nitrogen oxide generation which accelerates endothelialization after substrate healing of BHV.

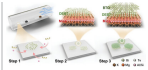
Abstract | Full text | PDF | References | Request permissions

Full Access

Buffer Layer Stabilized Single-Unit Cell Ferroelectric Bi_2TeO_5

Yunfei Li, Alei Li, Cong Wang, Mengjiao Han, Junlong Zhu, Yunlei Zhong, Pin Zhao, Ge Song, Shun Wang, Zongjie Shen, Lin Wang, Hui Zhang, Wu Zhou, Lu You, Wei Ji, Junhao Lin, Liuqi Kang

First Published: 23 December 2024



The growth of monolayer 2D Bi_2TeO_5 is achieved by introducing a buffer layer between the substrate and nanosheets, which relieves strain and stabilizes in-plane ferroelectricity. This method enhances the synthesis of monolayer nanosheets, establishes a viable approach for ultrathin ferroelectric materials, and has the potential to serve as a universal technique for synthesizing 2D ternary oxides.

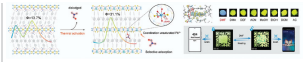
Abstract | Full text | PDF | References | Request permissions

Full Access

Direct Crystallographic Observation of Obvious Structural Deformation in a Lead Halide Framework Induced by Host–Guest Interactions

Xinfeng Chen, Quanzheng Deng, Shi Wang, Yichong Chen, Yukong Li, Wenyan Dan, Yang Liu, Yi-nan Wu, Lu Han, Honghan Fei

First Published: 23 December 2024



The crystallographic observation of obvious structural deformation in a lead bromide framework induced by the cleavage of solvent molecules, which significantly modulates the photophysical properties including enhanced self-trapped emission, is reported. The activated framework featuring an unsaturated coordination side of Pb^{2+} sites achieve selective and reversible binding with environmental N,N-dimethylformamide vapor, highlighting high potential in multilevel information encryption and anti-counterfeiting.

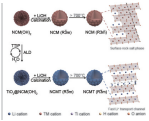
Abstract | Full text | PDF | References | Request permissions

Full Access

Pinning the Surface Layered Oxide Structure in High Temperature Calcination Using Conformal Atomic Layer Deposition Coating for Fast Charging Cathode

Xincan Cai, Pu Yan, Tianye Xie, Yifan Wu, Caihong Zheng, Rongliang Shang, Shuaishuai Yin, Yue Zhang, Fan Zheng, Xuerong Liu, Jin Xie

First Published: 29 December 2024



Atomic layer-deposited thin films on hydroxide precursors enable gradient doping during high-temperature solid-state lithiation, which reduces oxygen vacancies, prevents layered-oxide decomposition, and preserves Li^+ transport channels, thereby enhancing rate capability and cycle stability.

Abstract | Full text | PDF | References | Request permissions

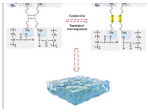
Full Access

A New Self-Healing Green Polymer Gel with Dynamic Networks for Flow Control in Harsh Reservoirs

Chuanhong Kang, Jixiang Guo, Wyclif Kiyingi, Jiao Li, Pengcheng Xue

First Published: 20 December 2024

A self-healing in situ crosslinked polymer hydrogel with dynamic covalent adaptive network is constructed by using cystine hydrochloride as raw material. The dynamic network is caused by the exchange of disulfide bonds, in which adjacent disulfide bonds change during breaking and formation. The dynamic network formed by topological network rearrangement makes the hydrogel have good toughness and self-healing peculiarity.



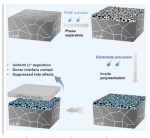
Abstract | Full text | PDF | References | Request permissions

Full Access

A Facile Humidity-Induced Porous Framework Filled with In Situ Initiated Gel Electrolyte for Stabilizing $Li_{1.4}Al_{0.4}Ti_{1.6}(PO_4)_3$/Li Interface

Dezhi Yang, Yanan Yang, Yiyang Sun, Tao Zhang

First Published: 23 December 2024



A facile composite interface layer composed of humidity-induced porous PVDF framework filled with in situ initiated poly(1,3-dioxolane)-based gel electrolyte is proposed to stabilize Li/ $Li_{1.4}Al_{0.4}Ti_{1.6}(PO_4)_3$/Li interface. The synergistic effect of physical isolation from the porous framework, superb stability to lithium metal by the GPE and alloy effect formed by the reduction of the initiator effectively improves the stability of $LiATiPO_4$ interface.

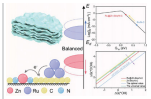
Abstract | Full text | PDF | References | Request permissions

Open Access

Synergistic Effects of Ruthenium and Zinc Active Sites Fine Tune the Electronic Structures of Augmented Electrocatalysis

Tingyu Lu, Jing Li, Jingwen Ying, Ningkang Peng, Linda Zhang, Yizhou Zhang, Di Zhang, Songbo Ye, Lin Xu, Dongmei Sun, Hao Li, Yanhui Gu, Yawen Tang

First Published: 23 December 2024



This study presents an electronic fine-tuning (EFT) strategy to optimize the electronic structures of Ru species and single-atom Zn sites by the virtue of layered nanosheets, significantly enhancing ORR and HER activities. Spectroscopic analysis and theoretical calculations uncover that this EFT effect breaks the ORR scaling limitation and positions closer to the top peak of the HER volcano model.

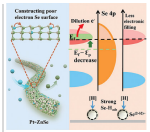
Abstract | Full text | PDF | References | Request permissions

Full Access

Diluting the Electric Supply of Surface Selenium Species to Realize Enhanced Hydrogen Monitoring in Agriculture

Xiaowu Wang, Zhigang Zeng, Zhiheng Ma, Muxen Li, Yin Wang, Zhanchen Wang, Ruiling Gao, Xin Jia, Pengfei Hu, Bo Lu, Zhenggang Xue, Jiaqiang Xu

First Published: 30 December 2024



An electron-dilution strategy is developed through doping Pt atoms on the surface of ZnSe NWs to realize electron-deficient Se sites and exhibit excellent H_2 sensing performances. Integrating the Pt-ZnSe MSMS sensors array into multifunctional wireless sensing device, it can realize real-time H_2 temperature/humidity monitoring and cloud data transmission for hydrogen agriculture.

Abstract | Full text | PDF | References | Request permissions

Full Access

First Published: 23 December 2024



In this work, a smart glove system based on the hydrogel triboelectric nanogenerator is proposed for person recognition and gesture control functionalities. Through the coordinated design of hardware-software architecture, the smart glove enables precise control of drone flight posture via contact sensing. Meanwhile, it leverages noncontact sensing to recognize personalized fingertip trajectories, enabling unlocking the aforementioned drone control interface.

Abstract | Full text | PDF | References | Request permissions

Full Access

Dynamic Convolutional Neural Networks Based on Adaptive 2D Memristors

Heemyoung Hong, Xi Chen, Woohyun Cho, Ho Yeon Yoo, Jaewhan Oh, Minseok Kim, Geunwoo Hwang, Yongsoo Yang, Linfeng Sun, Zhongrui Wang, Heejun Yang

First Published: 23 December 2024



The hardware-software co-designed solution is demonstrated, a dynamic Convolutional Neural Network (dCNN) empowered by three-terminal adaptive two-dimensional (2D) memristors. These memristors consist of a vertical heterostructure integrating silver, an atomically thin insulator ($CrPS_4$), and graphene as a gate-tunable semimetal. This configuration allows for the dynamic tuning of conductive filament properties, emulating the heterosynaptic plasticity observed in biological neural systems.

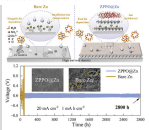
Abstract | Full text | PDF | References | Request permissions

Full Access

Kinetics-Mediating Artificial Interphase for Ultrafast Zn Metal Anodes

Qiaoyun Liu, Long Jiao, Jiahen Wang, Hongyuan Bai, Chao Yi, Yusen Fu, Jiajia Liu, Chuang Wang, Yachen Lei, Tian Zhang, Leixin Yang, Dengkun Shu, Shuo Yang, Chenyang Li, Huan Li, Wenjun Zhang, Bowen Cheng

First Published: 23 December 2024



An in situ crafted amorphous zinc pyrophosphate (ZPPO) interphase with consecutive kinetics-mediating effect is proposed to realize superior cycling stability of Zn metal anodes. This designed interphase can not only drive homogeneous ion diffusion and high Zn^{2+} enrichment, but also lower the Gibbs free energy of Zn^{2+} deposition, thus achieving dendrite-free and kinetics-boosted Zn electrodeposition under high current rates.

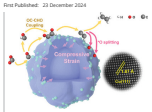
Abstract | Full text | PDF | References | Request permissions

Full Access

Photoinduced Lattice Compression of Cu for Enhanced Production of Ethylene from CO_2

Zhenyao Li, Wei Wei, Xuli Hu, Zhen Zhang, Yangchun Hu, Yushan Wu, Yao Wang, Junchen Xu, Mingyue Ding

First Published: 23 December 2024



By irradiating the photosensitive Cu sol-gel in UV, the *–CuJ4cat can be formed, and exerts compressive strain to the Cu(111) lattice. The compressed Cu(111) lattice exhibits lower surface energy and lower C···C coupling free energy, and facilitates spontaneous *O splitting immediately after the C···C coupling process to produce *CCH, enabling enhanced C_2H_4 production.

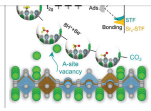
Abstract | Full text | PDF | References | Request permissions

Full Access

Modulating e_g Occupancy by A-Site Vacancy to Boost Photocatalytic CO_2 Reduction on Perovskite Oxides

Yibo Gao, Miaomiao Zhang, Zutao Fan, Yang Jin, Zhanlong Song, Wenlong Wang, Xiqiang Zhao, Yanpeng Mao

First Published: 16 January 2025



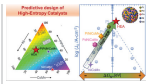
Abstract | Full text | PDF | References | Request permissions

Full Access

Design and Synthesis of PtPdNiCoMn High-Entropy Alloy Electrocatalyst for Enhanced Alkaline Hydrogen Evolution Reaction: A Theoretically Supported Predictive Design Approach

Athira Chandran M, Pritha Dutta, Prashant Singh, Ashutosh K Singh, Bhagavatula L. V. Prasad

First Published: 29 December 2024



A new screening guideline for the down-selection of PtPdNiCoMn high-entropy alloy (HEA) electrocatalyst for hydrogen evolution reaction based on a possible range of variance in bond length. The HEA has a medium TM-H surface bonding. The Volcano plot shows that the HEA is at the apex with the near-zero ΔG_{H^*} and highest exchange current density.

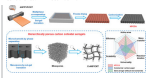
Abstract | Full text | PDF | References | Request permissions

Full Access

Hierarchically Porous Carbon Colloidal Aerogels for Highly Efficient Flow Cells

Yinglai Hou, Zhizhi Sheng, Mengchuang Zhang, Kaifa Lin, Jie Kong, Xuelong Zhang

First Published: 24 December 2024



Hierarchically porous carbon colloidal aerogels (HPCCA) are exploited using a sol-gel transition method together with a multiphase co-separation strategy, enabling highly efficient mass transfer and high redox activity. This work offers a new chemistry paradigm for developing advanced aerogel materials and sheds light on high-performance flow electrochemical devices.

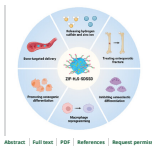
Abstract | Full text | PDF | References | Request permissions

Full Access

A Bone-Targeting Hydrogen Sulfide Delivery System for Treatment of Osteoporotic Fracture via Macrophage Reprogramming and Osteoblast-Osteoclast Coupling

Yi Qin, Zhen Zhang, Xiaobin Guo, Wenhao Li, Wenyu Xie, Gaoran Ge, Yanyue Li, Min Guan, Ang Gao, Lu Mao, Huaiyu Wang, Paul K. Chu, Dechun Geng

First Published: 23 December 2024



Bone-targeting ZIF-H_2S-SDSD nanoparticles release H_2S in bone tissues without affecting the serum H_2S level, thereby mitigating potential risks of systematic H_2S delivery. The synergistic effects of released Zn^{2+} and H_2S promote macrophage metabolic reprogramming and regulate osteoblast-osteoclast coupling. ZIF-H2S-SDSD nanoparticles simultaneously promote fracture healing and alleviate osteoporosis, holding great promise in the clinical treatment of osteoporotic fracture.

Abstract | Full text | PDF | References | Request permissions

Full Access

Nature-Inspired Design of Twisted MXene Heating Wires for Robust Wearable Heating Textiles

Woojae Jeong, Hwansoo Shin, Hanseul Nam, Hyundae Cho, Jeongbin Heo, Jaesik Seo, Tae-Hee Han

First Published: 19 December 2024



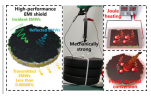
Abstract | Full text | PDF | References | Request permissions

Full Access

High-Performance Multifunctional Nanopapers with Superior Mechanical Strength, Electromagnetic Interference Shielding, and Thermal Management for Next-Generation Electronics

Fugang Hu, Mengheng Li, Pengfei Li, Jinsong Zeng, Tianguang Wang, Jinpeng Li, Bin Wang, Chen Wu, Kefu Chen

First Published: 23 December 2024



Ultra-flexible, lightweight, and mechanically robust multifunctional nanopapers with sandwich-like layered structures, showcasing remarkable tensile strength (701.82 MPa), outstanding toughness (101.86 MJ m^{-3}), excellent EMI shielding (62.28 dB), and high Joule heating and photothermal conversion capabilities (242.78 °C). These properties make the nanopapers promising candidates for next-generation electronics and advanced thermal management systems.

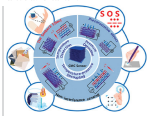
Abstract | Full text | PDF | References | Request permissions

Full Access

High-Performance Bimodal Temperature/Pressure Tactile Sensor Based on Lamellar CNT/MXene/Cellulose Nanofibers Aerogel with Enhanced Multifunctionality

Lin Tian, Fu-Lin Gao, Yu-Xiao Li, Zhi-Yue Yang, Xinghe Xu, Zhong-Zhen Yu, Jie Shang, Run-Wei Li, Xiaofang Li

First Published: 23 December 2024



In this study, a composite aerogel featuring a layered porous structure, characterized by ultra-low thermal conductivity and excellent electrical and thermoelectric properties, is developed to effectively monitor temperature and pressure stimuli. The sensor exhibits a temperature resolution of 0.03 K and a pressure resolution of 0.3 Pa, demonstrating high sensitivity (20.5 $\mu V K^{-1}$) and stable piezoresistive properties (~45.2% kPa^{-1}). Its multimodal sensing mechanism supports thermoelectric energy harvesting, material identification, information transmission, smart wearable devices, and human-computer interfaces, thereby significantly advancing the design and application of high-performance dual-mode tactile sensors.

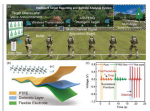
Abstract | Full text | PDF | References | Request permissions

Full Access

High-Accuracy Recognition Triboelectric Nanogenerator System for Shooting Report and Ballistic Analysis

Yanshuo Sun, Chengyu Li, Zijie Xu, Hengrui Sheng, Yusheng Wang, Erming Su, Zhong Lin Wang, Lao N.Y. Cao

First Published: 23 December 2024



A multifunctional intelligent target reporting and ballistic analysis system is innovatively proposed, aiming to solve the issues of existing systems: 1) Low accuracy in target reporting for extreme-shooting results; 2) Complexity and high error rate of ballistic analysis; 3) Single functionality and limited performance in extreme environments, achieving high precision in target reporting and the prediction of shooting positions.

Abstract | Full text | PDF | References | Request permissions

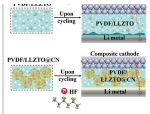
Full Access

Porous g-C_3N_4 Microspheres Wrapped by Garnet Nanoparticles Enable Solid Composite Electrolytes with Improved Ionic Conduction and Interfacial Stability

Wenjing Wang, Mengyang Jia, Zhijie Bi, Xiangxin Guo

First Published: 26 December 2024

LLZTO nanoparticles are confined into the porous g-C_3N_4 microspheres via the metal-nitrogen bonding, and 3D LLZTO frameworks with continuous and fast ionic transfer channels are thus constructed inside composite electrolytes. The introduction of g-C_3N_4 in electrolytes promotes the formation of a Li_3N-enriched SEI and suppresses the side reaction between PVDF and Li-metal, leading to enhanced cycle stability of cells.



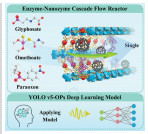
Abstract | Full text | PDF | References | Request permissions

Full Access

Enzyme-Nanozyme Cascade Flow Reactor Synergy with Deep Learning for Differentiation and Point-of-Care Testing of Multiple Organophosphorus Pesticides

Yujiao Bai, Shun Nie, Wenqing Gao, Nianqiang Li, Peihua Zhu, Lina Zhang, Jinghua Yu

First Published: 26 December 2024



An AChE/C_{60}@MOF-545-Fe enzyme-nanozyme flow reactor is constructed for detecting various OPs, and a smartphone-based POCT platform is successfully built by integrating a self-developed deep learning model to track the degradation process of OPs in real samples. This provides a promising strategy for pollutant detection and opens a new path for flow reactor design.

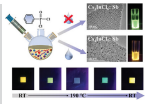
Abstract | Full text | PDF | References | Request permissions

Full Access

Hydrolysis Reaction-Induced Phase Regulation of Sb-doped Zero-Dimensional Perovskite $Cs_3In_2Cl_9$ Nanocrystals for Optoelectronic and Information Encryption Applications

Junchun Li, Zengze Liu, Guoqing Tong, Baochang Wang, Hongtao Zhu, Lin Shi, Yanpeng Gao, Ping Chen, Yang Jiang

First Published: 30 December 2024



The phase-controlled synthesis of 0D perovskite $Cs_3In_2Cl_9$ Sb nanocrystals is achieved by manipulating the H_2O addition. While $Cs_3In_2Cl_9$ Sb crystallizes as Cs_3InCl_9: Sb without H_2O, the H_2O addition induces the hydrolysis of chlorine source ($PrPrOCl_2$) and subsequently promotes the formation of Cs_3InCl_9: Sb. Moreover, a reversible phase transition between $Cs_3In_2Cl_9$: Sb and Cs_3InCl_9: Sb can be realized through heating–cooling cycles.

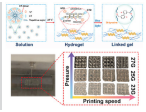
Abstract | Full text | PDF | References | Request permissions

Full Access

Rapidly Forming Recombinant Miniature Spidroins Hydrogels Composed of Nanofibrils with Tunable Mechanical Properties for Bio 3D Printing and Biomimetic Cellular Scaffolds

Cong Wang, Qi Zhang, Hanbai Wu, Shuai Zhang, Xiong Zhou, Min Li, Yuhan Chen, Wei Liu, Min Du, Jun Fan, Furong Chen, Jinlian Hu

First Published: 26 December 2024



In this paper, the mechanism of the formation of recombinant spidroins hydrogel with a tunable mechanical property under ambient condition is revealed. Spidroin aqueous solution undergoes β-sheet conversion from micelles to amyloid-like nanofibrils and further di-tyrosine crosslinking inducing gelation. Moreover, the spidroins hydrogel can be used for the bio 3D printing and biomimetic cellular scaffold.

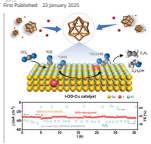
Abstract | Full text | PDF | References | Request permissions

Full Access

Trace Iodine Modified Copper Catalyst Drives Asymmetric C−C Coupling in Stable CO_2 Electroreduction

Zijun Yan, Min Liu, Zeyu Guo, Quhan Chen, Ziyun Xi, Xue-Zhong Sun, Jiahui Yu, Tao Wu

First Published: 23 January 2025



An electrocatalyst, I-OD-Cu_x is designed for CO_2 electroreduction, incorporating trace iodine doping and a Cu_2O hexapod-derived oxide structure. This configuration creates an active surface that enhances the adsorption of CO_2 and CO_2 facilitating the coupling of *CO and *CHO intermediates. Periodic iodine treatments effectively prevent catalyst agglomeration and preserve the iodine-modified active sites, ensuring improved catalytic stability for producing C_{2+} products.

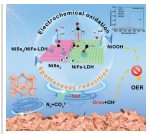
Abstract | Full text | PDF | References | Request permissions

Full Access

Mediating Self-Oxidation and Competitive Adsorption for Achieving High-Selective Urea Oxidation Catalysis at Industrial-Level Current Densities

Pengfei Qiao, Guorui Li, Xiuyan Xu, Danni Wang, Fangqing Wang, Liangliang Xu, Lingyu Lu, Hailin Cong, Mingliang Sun

First Published: 23 December 2024



The nanosheet-like NiS_x/NiFe-LDH catalyst with rich crystalline/amorphous heterointerface is developed to catalyze UOR. Such structure can restrain the self-oxidation reaction and boost the competitive adsorption of urea, which help to constrict the overaccumulation of NiOOH species and OH^- ions at NiS_x/NiFe-LDH surface during the UOR process, thereby achieving high UOR selectivity, activity, and long-term durability at industrial-level current densities.

Abstract | Full text | PDF | References | Request permissions

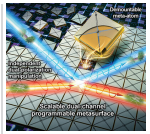
Editor's Choice

Full Access

Scalable and High-Isolation Dual-Channel Programmable Metasurface With Demountable Meta-Atom

Liang Xu, Xin Ge Zhang, Qi Yang Li, Dong Jie Wang, Tie Jun Cui, Wei Xiang Jiang

First Published: 23 December 2024



A unique meta-atom design method is proposed by embedding two varactors in stacked layers to generate high-isolation dual polarization channels. By arranging the demountable meta-atoms freely, a scalable dual-channel programmable metasurface is realized to control dual-polarized waves independently, even at large incident angles. This approach opens up avenues to develop low-crosstalk multiplexed programmable metasurfaces with high performance and stability.

Abstract | Full text | PDF | References | Request permissions

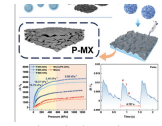
Full Access

Biomimetic Pyrolytic MXene-Based Multifunctional Films with Multi-Level Structure for Wearable Piezoresistive Devices and Bioelectronics

Zhaoling Huang, Chenggi Ge, Siyuan Li, Miao Cai, Yun Hui, Xinqin Liao, Qi Zeng

First Published: 23 December 2024

A bio-inspired MXene flexible film with a layered structure and a simple microfabrication strategy is proposed. The unique structure and processing scheme endow the novel sensor with exceptional sensitivity, a wide detection range, fast response and recovery times, and high cycling reliability. Additionally, it exhibits excellent charge storage and electron transport capabilities. This advancement facilitates the development of a new generation of multimodal wearable electronic devices, promising significant applications in medical diagnostics, electronic skin, and human-machine interaction.



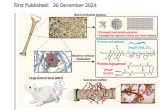
Abstract | Full text | PDF | References | Request permissions

Full Access

3D-Printed Dual-Bionic Scaffolds to Promote Osteoconductivity and Angiogenesis for Large Segment Bone Restoration

Bo Chen, Qi Chen, Haodong Zhang, Donghui Zhang, Cuidi Li, Ke Ma, Mengyue Dou, William Weijia Lu, Jin Qi, Lianfu Deng, Runhui Liu, Wenguo Cui

First Published: 26 December 2024



A dual-bionic 3D printed bredigite scaffold mimics bone structure and supports bioactivity. Its isotropic single-cell design adapts to load-bearing requirements and facilitates vessel and bone ingrowth. Functionalization with β-amino acid polymer $DM_{10}CO_{10}$ and deferoxamine enhances stem cell adhesion and vascularization. In a rat model, it showed exceptional osteoconductive and angiogenic properties for large bone defect repair.

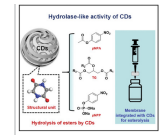
Abstract | Full text | PDF | References | Request permissions

Full Access

Carbon Dots with Polycyclic Dipeptide Structure Surpass Natural Hydrolase Performance

Mengling Zhang, Zeyu Wu, Yan Zhang, Tao Hu, Wenwen Li, Hui Huang, Mingwang Shao, Yang Liu, Xing Fan, Zhenhui Kang

First Published: 26 December 2024



Carbon dots (CDs) with polycyclic dipeptide structures have superior hydrolase-like performance. The highly efficient catalytic activity of CDs comes from their cyclic dipeptide structure, where the N in the cyclic dipeptide of CDs is the adsorption and active site for hydrolyzing esters. Besides, the CDs are used to construct a catalytic membrane that can be hydrolyzed instantaneously when esters pass through.

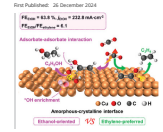
Abstract | Full text | PDF | References | Request permissions

Full Access

Preferentially Stabilizing the Watershed Intermediates by Adsorbate-adsorbate Interaction to Accelerate CO_2 Electroreduction to Ethanol

Pu Huang, Binglin He, Yuming Dong, Jing Zhou, Jing Xu, Changsi Pan, Yang Lou, Yao Wang, Ying Zhang, Hongwen Huang, Jiawei Zhang

First Published: 26 December 2024



CO_2 electroreduction to ethanol is accelerated via preferentially stabilizing the watershed intermediates ($^*CHCOH$) by intensifying surface-adsorbed hydroxyl species ($^*OH$) in the amorphous-crystalline interface to create adsorbate-adsorbate interaction.

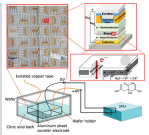
Abstract | Full text | PDF | References | Request permissions

Open Access

Organic Permeable Base Transistors—Reliable Large-Scale Anodization for High Frequency Devices

Amin Bonsi, Ghader Darbandy, Jan Frede, Moritz Flemming, Christian Matthus, Lautaro Petrauskas, Juan Wang, Kyung-Geun Lim, Hans Kleemann

First Published: 16 January 2025



Electrochemical anodization is optimized for organic permeable base transistors (OPBTs), achieving an unprecedented 87% yield and reproducibility for vertical organic transistors (VOTs) on a 15 × 15 cm wafer. Controlled #A base oxidation ensures a medium transconductance of 10^{-2} S, leakage current below 10^{-9} A, current gain of 10^6, and transit frequency up to 2.6 MHz V^{-1}, validated via TCAD simulations.

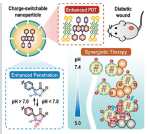
Abstract | Full text | PDF | References | Request permissions

Full Access

A pH-Responsive, Surface Charge-Switchable Nanosystem with Enhanced Biofilm Penetration for Synergistic Photodynamic and Antibiotic Therapy of Diabetic Wounds

Zhencheng Sun, Minghui Xiao, Shuqi Lu, Cheng Wang, Hao Fu, Liang Tian, Ling Shi, Chunlei Zhu

First Published: 29 December 2024



This study introduces an innovative approach for treating chronic wounds using pH-responsive, charge-switchable nanoparticles loaded with aggregation-induced emission photosensitizers and natural saturated fatty acids. By leveraging a unique charge reversal mechanism, these nanoparticles effectively penetrate biofilms, disrupt their structure, and enhance antibiotic action. The synergistic therapy significantly accelerates wound healing in diabetic models, paving the way for improved treatments.

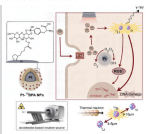
Abstract | Full text | PDF | References | Request permissions

Full Access

Boronophenylalanine-Functionalized Platinum Nanozymes Sensitizing Neutron Capture Therapy

Xiangxia Li, Guiyuan Chen, Bing Hong, Changqing Guo, Huanjun Zhu, Qilong Zhu, Yuanyu Liu, Zilong Li, Lingling Li, Chao Gao, Peng Lu, Dong Qian, Lizhen Liang, Yujie Xiong, Yuanzeng Min

First Published: 29 December 2024



Trehalose-modified boronated platinum nanoparticles enhance boronophenylalanine enrichment at tumor sites after systemic administration. Platinum catalyzes the increase in reactive oxygen species and, together with the production of high-energy particles after thermal neutron beam irradiation, causes enhanced DNA damage in tumor cells, thereby sensitizes them to BNCT.

Abstract | Full text | PDF | References | Request permissions

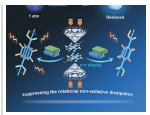
Full Access

Pressure Regulated π–π Slip Enabling Blue-Light Emission Enhancement of Terephthalic Acid

Qing Yang, Yixuan Wang, Guangming Niu, Laizhi Sui, Xinyi Yang, Bo Zou

First Published: 23 December 2024

Pressure engineering endows pressure-treated TPA with an enhanced rotational energy barrier of phenyl based on the slipped π–π stacking arrangement and enhanced hydrogen-bond interactions. This is advantageous for the suppression of non-radiative dissipation and promotes the harvest of high-performance blue-light emission with PLQY of 74.1%.



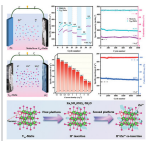
Abstract | Full text | PDF | References | Request permissions

Full Access

Vacancy Engineering on MnSe Cathode Enables High-Rate and Stable Zinc-Ion Storage

Wenqing Zhong, Rui Zhao, Yirong Zhu, Yuting Xu, Wenhao Chen, Chao Peng

First Published: 26 December 2024



A vacancy engineering strategy is utilized to design and synthesize the Se vacancies-rich MnSe microspheres (V_{Se}-MnSe) and employ them as cathode materials for ZIBs and ZICs for the first time. The V_{Se}-MnSe//Zn ZIBs achieve significantly enhanced specific capacity, rate performance, and cycling lifespan. Further, the V_{Se}-MnSe//PC ZICs show splendid electrochemical properties.

Abstract | Full text | PDF | References | Request permissions

Full Access

Pixel-Level Hardware Strategy for Large-Scale Convolution Calculation in Neuromorphic Devices

Xianghong Zhang, Di Liu, Jiamin Wu, Enping Cheng, Congyao Qin, Changsong Gao, Liuting Shan, Yi Zou, Yuanyuan Hu, Tailiang Guo, Huipeng Chen

First Published: 23 December 2024



Based on the dynamic change of electron concentration, a novel pixel-level hardware strategy is proposed to realize convolution calculation at a single device. This strategy provides a novel method to process extensive convolution operations with high resource utilization efficiency, advanced power efficiency, and fewer convergence cycles. As a basic universal strategy, this strategy can be extended to other neuromorphic devices.

Abstract | Full text | PDF | References | Request permissions

Full Access

A Precision Mo_2VC_x-Based Nanomedicine for Effective Cancer Elimination by Harnessing Senescence Induction and Immunogenic Response

Ruoxi Zhao, Lili Feng, Yanlin Zhu, Chenghao Yu, Mikhail V. Zyuzin, Shili Gai, Desheng Chen, Siming Zhang, Haixia Zhu, Piaoping Yang

First Published: 27 December 2024



A biometallic vanadium-based MXene nanoplatform (Mo_2VC_x-PalbocliB-RGD) is developed to combine pro-senescence therapy with nanozyme catalytic therapy to active immunotherapy. To prevent tumor cells growth and disrupt redox homeostasis through multi-enzyme cascade activity, and then successfully induce cancer cells senescence and apoptosis, activate the immune system, and ultimately suppress tumor growth.

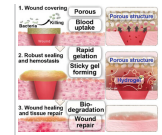
Abstract | Full text | PDF | References | Request permissions

Full Access

Porous Materials with Water-Triggered Instant Transformation to Robust Hydrogel Adhesives for Rapid Hemostasis of High-Pressure Hemorrhages

Guoqing Wang, Jianfei Wang, Xinping Wang, Yuanyuan Meng, Xiangzhen Feng, Gaoli Liu, Dong-An Wang, Changjiang Fan

First Published: 27 December 2024



Porous-solid materials with water-triggered rapid phase transformation into robust sticky hydrogels are developed with the proposed novel methodology, which combines the advantages of hemostatic sponges and hydrogel adhesives. As sealing strength can wet tissues reaches an amazing ≈600 mm·Hg, they readily achieve the sealing and hemostasis of the high-pressure, active bleeding wounds in pigs by simple in situ pressing.

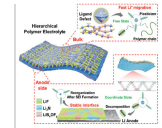
Abstract | Full text | PDF | References | Request permissions

Full Access

Decoupling Interfacial Stability and Ion Transport in Solid Polymer Electrolyte by Tailored Ligand Chemistry for Lithium Metal Battery

Ruilian Lv, Yingmin Jin, Yumeng Li, Mengyu Fu, Yuxin Gong, Lei Lei, Yong Zhang, Jijun Xu, Yueping Xiong

First Published: 29 December 2024



Here, hierarchical ligand-engineered University of Oslo (UiO) metal–organic framework is applied as regulation framework to develop spatially confined solvation structure for in situ polymerized solid electrolyte, which establishes fast Li^+ migration structure for bulk phase electrolyte and realizes the anion-derived solid electrolyte interphase configuration simultaneously through hierarchical ion-coordination design.

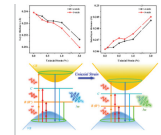
Abstract | Full text | PDF | References | Request permissions

Full Access

Strain Control of Third Harmonic Generation in Nb_2SiTe_4 Driven by Tuneable Anisotropic Characteristics

Yihang Ouyang, Jin Dai, Zhenzhen Wan, Wenzhe Zhou, Tao Xu, Kostya S. Novoselov, Maciej Koperski, Zhihui Chen, Jun He

First Published: 26 December 2024



The strain control of nonlinear optical effects in Nb_2SiTe_4 characterized by in-plane anisotropy is investigated. A record high third-order susceptibility of 2.43×10^{-18} m^2/V^2 is obtained through the interband resonance of the third harmonic generation. By the application of uniaxial strains along the principal axes, the anisotropy of Nb_2SiTe_4 can be tuned into different regimes.

Abstract | Full text | PDF | References | Request permissions

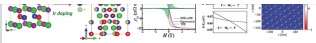
Editor's Choice

Full Access

Giant Topological Hall Effect in Magnetic Weyl Metal $Mn_3Pd_{0.5}Pr_{0.5}Sn$

Arnab Bhattacharya, Sreeparvathy PC, Athar Ahmed, Daichi Kurebayashi, Oleg A. Tretiakov, Biswarup Satpati, Samik DuttaGupta, Aftab Alam, I. Das

First Published: 08 January 2025



Topologically safeguarded magnetic order is realized in the Weyl metallic Heusler alloy Mn2PdIr.5In0.5Sn, possessing non-centrosymmetric D2d symmetry and strong spin-orbit coupling. First-principles calculations reveal Weyl node pairs near the Fermi level. The material exhibits a large topological Hall effect, robust even at room temperature, and micromagnetic simulations predict an antiskyrmion lattice, highlighting the potential for spintronic applications.

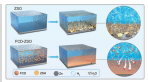
Abstract | Full text | PDF | References | Request permissions

Full Access

Suppressing Zinc Metal Corrosion by an Effective and Durable Corrosion Inhibitor for Stable Aqueous Zinc Batteries

Baohui Ren, Xiangyang Zhang, Hua Wei, Jingjing Jiang, Guangming Chen, Honghe Li, Zhuoxin Liu

First Published: 26 December 2024



This study introduces fucoidan (FCD), a green and cost-effective corrosion inhibitor, to mitigate the corrosion-related challenges in zinc metal anodes. FCD forms a robust, covalently bonded ultrathin protective layer on the zinc surface, effectively shielding the zinc from corrosive electrolytes and promoting uniform zinc deposition. The resultant zinc batteries demonstrate exceptional electrochemical stability and promising scalability.

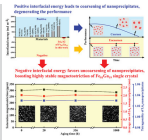
Abstract | Full text | PDF | References | Request permissions

Full Access

Highly Stable Magnetostriction in Nanoheterogeneous $Fe_{81}Ga_{19}$ Alloy Enabled by Uncoarsening of Nanoprecipitates Due to Negative Interfacial Energy

Boying Qiao, Shuoyu Zhao, Jichao Yao, Keyu Yan, Xiang Feng, Jingmin Wang, Dazhuang Kang, Jinghua Liu, Jiaxiang Shang, Qianfan Zhang, Yuye Wu, Wei Zhan, Ruiqiang Chen, Changbao Jiang

First Published: 24 December 2024



The high-performance nanoheterogeneous materials face a bottleneck of coarsening of nanoprecipitates caused by positive interfacial energy, leading to degeneration of performance. Here, in a $Fe_{81}Ga_{19}$ single crystal uncoarsening of the $L6_0$ nanoprecipitates boost is reported from the surprisingly negative interfacial energy. Consequently, highly stable magnetostriction is achieved. This work provides a promising strategy for developing highly stable nanoheterogeneous materials.

Abstract | Full text | PDF | References | Request permissions

Sign up for email alerts

Enter your email to receive alerts when new articles and issues are published.

Email address

Enter email

Continue

Journal Metrics

ADVANCED SCIENCE NEWS



Related Titles

- Advanced Healthcare Materials
- Advanced Intelligent Systems
- Advanced Materials
- Advanced Materials Interfaces
- Advanced Materials Technologies
- Advanced Science
- Angewandte Chemie
- Journal of the American Ceramic Society
- Laser & Photonics Reviews
- Macromolecular Rapid Communications
- physica status solidi (RRL)
- Small



© 2025 Advanced journals portfolio

ABOUT WILEY ONLINE LIBRARY
Privacy Policy
Terms of Use
About Cookies
Manage Cookies
Accessibility
Wiley Research DE&I Statement and Publishing Policies

HELP & SUPPORT
Contact Us
Training and Support
DMCA & Reporting Piracy

OPPORTUNITIES
Subscription Agents
Advertisers & Corporate Partners

CONNECT WITH WILEY
The Wiley Network
Wiley Press Room

Copyright © 1999-2025 John Wiley & Sons, Inc or related companies. All rights reserved, including rights for text and data mining and training of artificial intelligence technologies or similar technologies.

Check for updates

ADVANCED FUNCTIONAL MATERIALS
www.afm-journal.de

Carbon Dots with Polycyclic Dipeptide Structure Surpass Natural Hydrolase Performance

Mengling Zhang, Zeyu Wu, Yan Zhang, Tao Hu, Wenwen Li, Hui Huang, Mingwang Shao, Yang Liu,* Xing Fan,* and Zhenhui Kang**

Nature enzymes always suffer from high costs, harsh conditions, and instability, while, artificial one offers possibilities for addressing current challenges and plays a significant role in future industrial production. Here, the carbon dots (CDs), with well-defined polycyclic dipeptide structures, are reported to exhibit superior hydrolase-like catalytic performance beyond those of natural enzymes. Compared to natural lipase, the obtained CDs not only exhibit superior catalytic activity (2.85 times increase in V_m) but also have a broader range of substrate concentrations (0–8.0 mM) and substrate types (fatty ester, aromatic ester, phosphate ester), along with simpler catalytic conditions and superior stability. The highly efficient catalytic activity of CDs is attributed to the low activation energy of the reaction (E_a: 13.74 kJ mol^{-1}) and strong adsorption to the substrates. The results of theoretical calculations and comparative experiments demonstrate that the adsorption sites of CDs are located on the nitrogen atoms of the polycyclic dipeptide. Furthermore, a membrane integrated with CDs (membrane-catalyst) is constructed, through which the instantaneous hydrolysis of esters can be realized. This work provides new insight into the enzyme-like catalytic mechanisms of CDs and offers a new approach to designing enzyme-like materials with high performance.

1. Introduction

Hydrolysis reactions, catalyzed by hydrolases, are not only indispensable in daily life, such as improving food adaptability through lactose hydrolysis in food processing and enhancing household hygiene with enzymatic cleaning agents,[1,2] but also significantly impact industrial production efficiency and environmental protection.[3–6] Natural enzymes are efficient and specific, while their industrial applications are often limited by factors such as poor stability and high costs.[7] The artificial enzyme catalysts can not only mimic the catalytic activity and selectivity of natural enzymes but also achieve higher stability, stronger tolerance, and lower costs through molecular design and engineering modifications.[7–9] Recently, a variety of catalytically active hydrolase-like materials have been developed, including peptide-based enzymes,[10,11] molecularly imprinted polymers[12–14] and functional nanomaterials.[7,8,15–17] Among them, nanomaterials, such as metal/metal oxide nanoparticles,[15] metal organic framework[16] and carbon-based nanomaterials (like graphene oxide,[17]) have attracted significant attention due to their unique physicochemical properties. Those nanomaterials with hydrolase-like activity still face numerous challenges, with key areas for breakthroughs including: improving catalytic efficiency and selectivity, enhancing stability under extreme conditions, reducing production costs, and developing catalytic devices integrated with catalysts.[7,10] Notably, a deeper understanding of the catalytic mechanisms of these materials and optimizing their structural design are the most urgent scientific task toward their practical application.

Carbon dots (CDs) are one kind of carbon-based nanomaterials, and exhibit remarkable advantages and vast potentials in the field of bio-catalysis.[18,19] They have not only been proven to enhance the catalytic activity and stability of natural enzymes through modification or immobilization,[20,21] but they have also been shown to mimic the catalytic activity of natural enzymes.[22–27] At present, many enzyme-like activities of CDs (such as peroxidase,[22–24] catalase,[23,24] oxidase,[25,26] superoxide dismutase[23,27] have been reported, while there is few reports on hydrolase-like activitiy of CDs.[28] Compared with other

M. Zhang, Z. Wu, Y. Zhang, T. Hu, W. Li, H. Huang, M. Shao, Y. Liu, Z. Kang
Jiangsu Key Laboratory for Carbon-based Functional Materials and Devices
Institute of Functional Nano and Soft Materials (FUNSOM)
Soochow University
Suzhou 215123, China
E-mail: hhuang0618@suda.edu.cn; yangl@suda.edu.cn; zhkang@suda.edu.cn

X. Fan
Research Center for Carbon-based Electronics and Key Laboratory for the Physics and Chemistry of Nanodevices
School of Electronics
Peking University
Beijing 100871, China
E-mail: xingf@pku.edu.cn

Z. Kang
Macao Institute of Materials Science and Engineering (MIMSE)
MUST-SUDA Joint Research Center for Advanced Functional Materials
Macau University of Science and Technology
Taipa, Macao 999078, China

The ORCID identification number(s) for the author(s) of this article can be found under https://doi.org/10.1002/adfm.202423470

DOI: 10.1002/adfm.202423470

 © 2024 Wiley-VCH GmbH

nanomaterials that have been found to show hydrolyzase-like activity,[7,8,29–31] CDs possess numerous advantages. First, CDs have a wide range of sources and easy to preparation, while their surfaces are rich in functional groups, making them easy to modify functionally and optimize catalytic efficiency and specificity. Besides, CDs have benign chemical and thermal stability, maintaining catalytic activity under various environmental conditions. Moreover, the low toxicity and good biocompatibility of CDs make them attractive for biological applications. Therefore, CDs are well candidates for developing hydrolase-like nanomaterials with high performance. Furthermore, it is worth mentioning that CDs with well-defined structures can serve as a foundation for the rational design of biocatalysts and the clarification of their catalytic mechanism.

Herein, we demonstrate that CDs with polycyclic dipeptide structure show hydrolase-like activitiy with high efficiency. The incorporation of specific cyclic dipeptide structures within the design of CDs can significantly enhance their enzyme-like activity. Cyclic dipeptide can serve as building blocks that provide specific functional groups conducive to catalytic actions. Furthermore, the spatial arrangement of polycyclic dipeptide can influence the active sites' accessibility, ultimately affecting substrate binding and conversion rates. In this work, the interaction of the obtained CDs on small molecule esters 4-nitrophenyl acetate (*p*NPA) was analyzed. Then, using the hydrolysis of *p*NPA as an example, the hydrolase-like catalytic activity and reaction kinetics of CDs were investigated, and the catalytic activity, suitable substrate concentration range, substrate range, and catalytic stability of CDs were compared with those of natural hydrolase. Based on the outstanding catalytic performance of CDs, the CDs integrated membrane catalyst was constructed. Finally, the active site and catalytic mechanism of the CDs were elucidated. This work not only develops a new approach for the design of artificial enzyme with hydrolase-like activitiy, but also provides deeper insight into the catalytic mechanism of carbon-based nanozymes.

2. Results and Discussion

2.1. The Interaction Between CDs and 4-Nitrophenyl Acetate

CDs were synthesized by the electro-polymerization method using serine as the raw material, as referred to in previous work by our group.[26] After four main steps (adsorption, electrooxidation, polymerization, and chain extension), serine polymerized to form CDs with cyclic dipeptide structure. Transmission electron microscopy (TEM) image revealed that the CDs exhibit a typical spherical morphology (**Figure 1a**), with average diameters ranging from 2 to 6 nm. The DLS measurement for the size distribution of CDs (Figure S1, Supporting Information) is in accordance with the TEM results. Besides, the zeta potential of CDs is -6.23 mV. The UV–Vis absorption spectrum (Figure S2, Supporting Information) of the CDs displays distinct absorption bands at 204 and 296 nm, attributing to the π-π* transition and the n-π* transition, respectively.[32,33] X-ray photoelectron spectroscopy (XPS) was also used for investigating the elemental compositions and structure of the CDs. As shown in Figure S3 (Supporting Information), the high-resolution C 1s XPS analysis of the CDs revealed three peaks at 284.7 eV (C—C), 285.9 eV (C—O/C—N), and 288.2 eV (C═O).[26,34] High-resolution N 1s XPS spectrum shows two peaks for the CDs, which are attributed to —NH_2/—NH— at 399.6 eV and C—N—C at 401.4 eV.[35] In the previous works, we demonstrated that the CDs electropolymerized from serine are composed of chain entanglements formed by the polymerization of cyclic dipeptides (as shown in Figure 1b),[26] and their sizes could be regulated by controlling the electrolysis parameters.[36] Since the structure of the CDs has been analyzed in detail in our previous work, the structural characterization of them will not be discussed in detail in this work. The specific synthesis mechanism and structural analysis of the CDs can be found in our previous article.[26]

Based on the clear structure of the CDs, we investigated the adsorption of the CDs to ester molecules for analyzing whether the CDs can be used for the hydrolysis of the ester. Using acetic acid as a model molecule, theoretical calculations were adopted to analyze the interaction between CDs and 4-nitrophenyl acetate (*p*NPA). One cyclic peptide chain of the CDs was used to represent the CDs. As shown in Figure 1c, the CDs are connected to the substrate mainly by hydrogen bonds, and the adsorption site is located on the nitrogen atom of the cyclic dipeptide. In addition, when *p*NPA is adsorbed on the CDs, its ester bond lengthens (from 1.379 to 1.396 Å), demonstrating that the ester bond is more easily broken after the ester substrate is adsorbed on the surface of the CDs. Fourier transform infrared (FTIR) spectrum was also utilized to analyze their interaction. For the CDs, the FTIR spectrum (Figure 1d) shows a broad band at 3448 cm^{-1}, indicating the stretching vibrations of O–H and N–H.[26] Furthermore, the peak at 1639 cm^{-1} in the CDs is associated with C═O bonds.[26,37] Additionally, the peaks located at 1386 and 1098 cm^{-1} in the FTIR spectrum of CDs correspond to the vibrations of C—N and C—O bonds.[26,38] However, after adding *p*NPA to the CDs, the characteristic signal of N–H from CDs (3448 cm^{-1}) is shifted to 3198 cm^{-1}, which is due to the formation of a hydrogen bond between the CDs and *p*NPA.[39] Both experimental and theoretical results show that the CDs are mainly adsorbed with the ester through hydrogen bonds.

2.2. The Catalytic Kinetic of CDs Toward the Hydrolysis of *p*NPA

Next, the CDs exhibited hydrolase-like catalytic activities were investigated. *p*NPA is a good substrate for examining the catalytic activity of hydrolase-like material because their catalytic activity can be easily detected by measuring the absorption of the hydrolysates (4-Nitrophenol, *p*NP). As shown in **Figure 2a**, *p*NPA can be catalyzed by CDs to form acetic acid (AcOH) and yellow *p*NP, and the product of *p*NP has an absorption peak located at 405 nm, as measured by UV-Vis spectroscopy (Figure 2b). The absorption spectra of the yellow product *p*NP catalyzed by CDs (60 μg mL^{-1}) at different reaction times were measured (0-20 min), and the absorption peak from *p*NP gradually increased with the extension of the reaction time. Since the OD_{405} signal is directly proportional to the *p*NP concentration, we subsequently converted its concentration and calculated the catalytic activity of the CDs using the *p*NP standard curve (Figure S4b, Supporting Information) recorded by a multifunctional microplate reader. As shown in Figure 2c, which displays the curves of product

© 2024 Wiley-VCH GmbH

16163028, 2025, 17, Downloaded from https://advanced.onlinelibrary.wiley.com/doi/10.1002/adfm.202423470 by Soochow University, Wiley Online Library on [04/06/2025]. See the Terms and Conditions (https://onlinelibrary.wiley.com/terms-and-conditions) on Wiley Online Library for rules of use; OA articles are governed by the applicable Creative Commons License

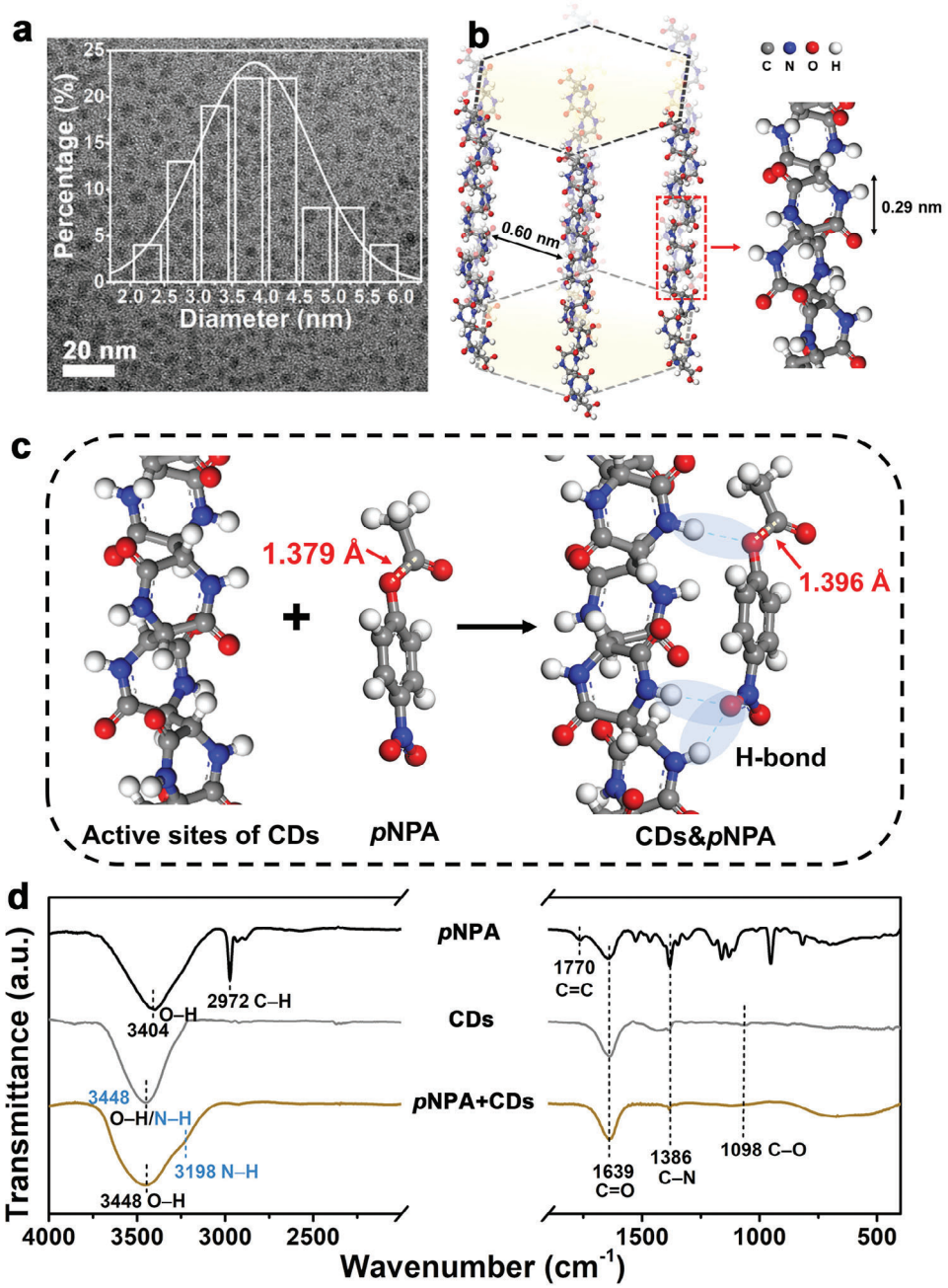


Figure 1. a) TEM image and size distribution (inset) of CDs; b) The schematic diagram of a unit structure for CDs; c) The adsorption and interaction of CDs chain with 4-nitrophenyl acetate (*p*NPA); d) FTIR spectra of *p*NPA, CDs, *p*NPA + CDs.

concentrations catalyzed by different concentrations of CDs (20–100 μg mL^{-1}) over time, the hydrolase-like activity of the CDs was found to be concentration-dependent.

In addition, the catalytic activities of CDs (60 μg mL^{-1}) in different concentrations of *p*NPA were measured. As shown in Figure 2d and Figure S5 (Supporting Information), when the *p*NPA concentration is in the range of 0–2 mM, the catalytic activity of CDs is linearly related to the *p*NPA concentration, following the characteristic of a first-order reaction ($v = kC^1$). In the range of 2–8 mM for *p*NPA concentration, the catalytic reaction kinetics of CDs show the characteristic between zero-order and first-order reactions ($v = kC^n$ (n = 0–1)), while, when the substrate concentration is greater than 8 mM, the catalytic activity of CDs is no longer affected by the substrate concentration, and the reaction follows are zero-order kinetics ($v = kC^0$). Moreover, we measured the catalytic activity of CDs (60 μg mL^{-1}) at different temperatures and calculated the activation energy (E_a) of the reaction system according to the Arrhenius equation (*p*NPA concentration: 2 mM). The E_a of the reaction system catalyzed by the CDs is 13.74 kJ mol^{-1} (Figure 2e). Such a small E_a proves that

© 2024 Wiley-VCH GmbH

16163028, 2025, 17, Downloaded from https://advanced.onlinelibrary.wiley.com/doi/10.1002/adfm.202423470 by Soochow University, Wiley Online Library on [04/06/2025]. See the Terms and Conditions (https://onlinelibrary.wiley.com/terms-and-conditions) on Wiley Online Library for rules of use; OA articles are governed by the applicable Creative Commons License

16163028, 2025, 17, Downloaded from https://advanced.onlinelibrary.wiley.com/doi/10.1002/adfm.202423470 by Soochow University, Wiley Online Library on [04/06/2025]. See the Terms and Conditions (https://onlinelibrary.wiley.com/terms-and-conditions) on Wiley Online Library for rules of use; OA articles are governed by the applicable Creative Commons License

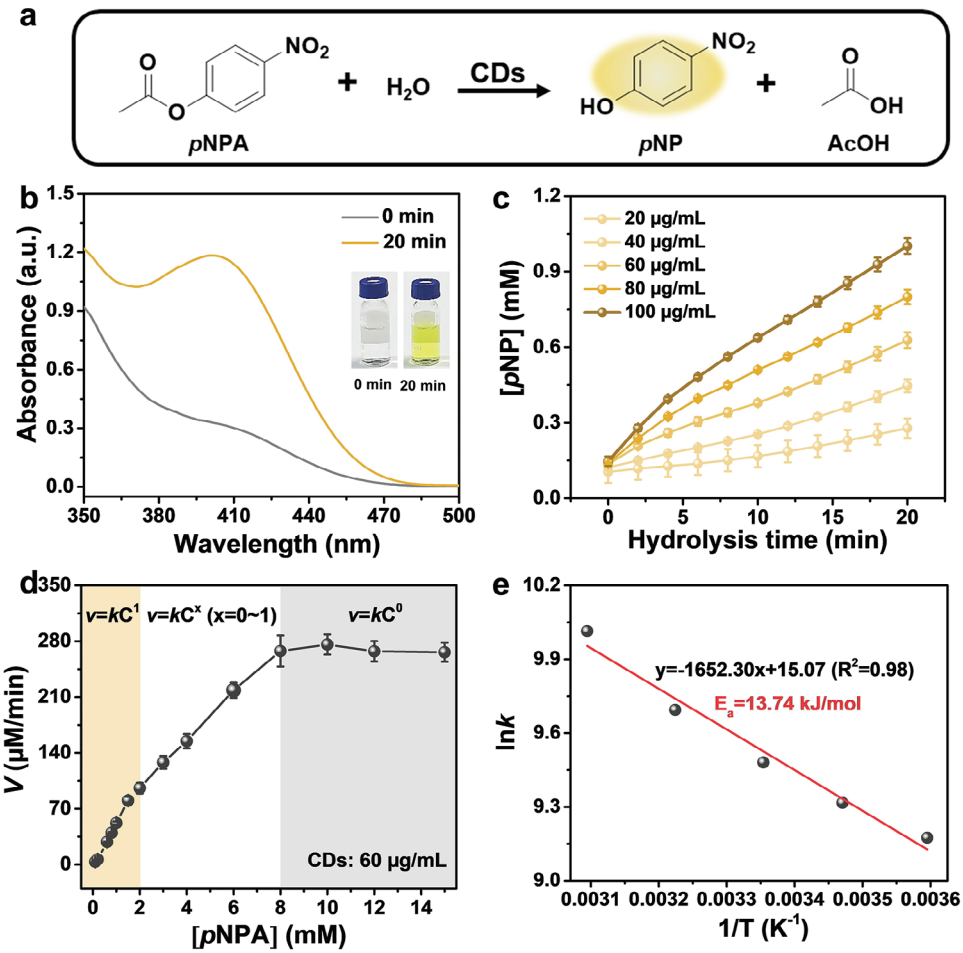


Figure 2. a) Schematic diagram of *p*NPA hydrolysis by CDs; b) UV–Vis absorption spectra of reaction system before and after catalyzed by CDs; c) Curves of product concentrations catalyzed by CDs with different concentrations (20-100 μg mL^{-1}) against time; d) The reaction kinetics for the CDs in different concentrations of pNPA (0–15 мм); e) The activation energy of CDs for *p*NPA hydrolysis (*p*NPA: 2 мм; in H_2O (pH = 6.76); 37 °C).

the CDs could have a high catalytic activity for the hydrolysis of esters.

2.3. The Comparison of Catalytic Performances Between CDs and Lipase

Based on the above analysis, it is found that the obtained CDs have hydrolyzase-like catalytic activity and low E_a. In the following experiments, we compared the catalytic activity and stability of CDs and natural lipase (from *Aspergillus oryzae*). As shown in **Figures** 3a and S6 (Supporting Information), both the CDs and lipase display high catalytic activity toward the hydrolysis of 4-Nitrophenyl acetate in phosphate buffered saline (PBS, 0.01 м, pH = 7.00). However, the CDs show outstanding catalytic ability than that of natural lipase in H_2O, where lipase could not catalyze the hydrolysis of 4-Nitrophenyl acetate in H_2O. Besides, CDs with different concentrations (20-100 μg mL^{-1}) in H_2O exhibit superior catalytic activity compared with lipase in PBS (Figure 3b). The kinetics of CDs in H_2O (60 μg mL^{-1}) and natural lipase in PBS (0.01 м, pH = 7.00) were analyzed. As shown in Figure 3c, the CDs show a wider range of suitable catalytic substrate concentration (*p*NPA: 0–8 мм) and a higher maximum reaction rate (Vm: 268 μм min^{-1}), compared with lipase (*p*NPA: 0–3 мм; Vm: 94 μм min^{-1}). Besides, both CDs and lipase follow the Michaelis-Menten equation within the tested concentration range (0–3 мм), as shown in Figure 3d. Through Lineweaver-Burk double reciprocal plots, the kinetic parameters including the values of maximum initial velocity (V_{max}) and Michaelis–Menten constant (K_m) were obtained, where the V_{max} and K_m values for the CDs are 1.68 мм min^{-1} and 21.52 мм, while those of the lipase are 0.43 мм min^{-1} and 5.32 мм. In comparison, although the adsorption capacity of CDs to substrates is weaker than that of natural enzymes, CDs exhibit higher catalytic efficiency than lipase as proved by the V_{max} values.

Considering the specificity of the enzyme to the substrate, we also tested the catalytic activity of CDs for different substrates, and compared their catalytic activity with that of lipase from different sources. Figure S7 (Supporting Information) shows the catalytic reaction curve of CDs toward different aromatic esters (a-d: 4-Nitrophenyl formate, *p*NPA, 4-Nitrophenyl butyrate, 4-Nitrophenyl pentanoate). As the side chain of aromatic ester increases, the catalytic rate of CDs gradually slows

 © 2024 Wiley-VCH GmbH

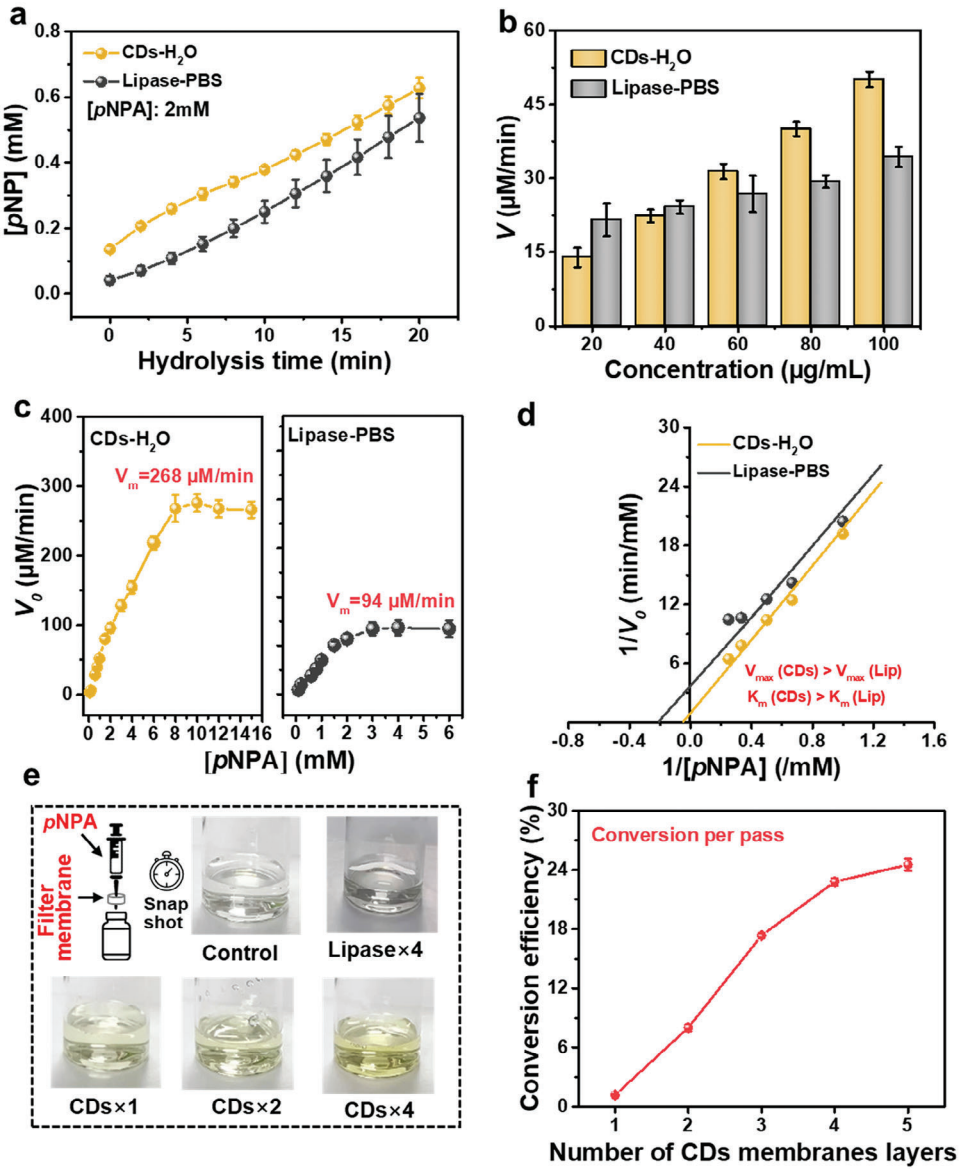


Figure 3. a) Curves of product concentrations against time catalyzed by CDs (60 μg mL^{-1}, in H_2O, pH = 6.76) and lipase (60 μg mL^{-1}, in PBS, 0.01 M, pH = 7.00); b) The catalytic activities of CDs and lipase with different concentrations (20–100 μg mL^{-1}) in H_2O (pH = 6.76) and PBS (0.01 M, pH = 7.00), the concentration of pNPA is 2 mM; c) Kinetics for hydrolytic activities of CDs and lipase (60 μg mL^{-1}) in H_2O (pH = 6.76) and PBS (0.01 M, pH = 7.00); d) Lineweaver-Burk plots of CDs and lipase (60 μg mL^{-1}); e) *p*NPA hydrolysis using CDs or lipase integrated membranes (control: blank membrane; CDs×1/2/4: 1/2/4 layers of membrane integrated with CDs; lipase×4: 4 layers of membrane integrated with lipase (*p*NPA: 2 mM); f) The single-pass conversion efficiency of CDs-integrated membranes with different number of layers.

down, which may be related to the side chain affecting the adsorption of the substrate onto CDs. The catalytic rates of CDs are 79.88, 31.68, 17.03, 1.34 μM min^{-1} toward 4-Nitrophenyl formate, *p*NPA, 4-Nitrophenyl butyrate, 4-Nitrophenyl pentanoate (as shown in Table S1, Supporting Information). Besides, other substrates (olive oil and phosphate ester) were used for evaluating the catalytic activity of CDs and lipase (from *Aspergillus oryzae*), as shown in Figure S8 (Supporting Information). For olive oil as substrate, CDs show similar catalytic activity with lipase under the same catalytic concentration (catalyst concentration: 20-100 μg mL^{-1}, lipase: in 0.01 M PBS (pH = 7), CDs: in H_2O). However, for phosphate ester, CDs have the catalytic ability to catalyze phosphate ester to *p*NP (catalytic rate: 13.58 μM min^{-1}), while the lipase did not show any catalytic activity. This shows that CDs have a wider range of substrate types than lipase. Furthermore, the catalytic activities of CDs and lipases from different sources (Lipase-1, Lipase-2, and Lipase-3: from *Aspergillus oryzae, Candida*, and pig pancreas) were investigated as well. As shown in Figure S9 and Table S1 (Supporting Information), the catalytic rates of CDs, Lipase-1, Lipase-2, and Lipase-3 (catalyst concentration: 60 μg mL^{-1}) are 31.68, 26.83, 16.17, and 19.14, respectively. Compared with these lipases from

© 2024 Wiley-VCH GmbH

16163028, 2025, 17, Downloaded from https://advanced.onlinelibrary.wiley.com/doi/10.1002/adfm.202423470 by Soochow University, Wiley Online Library on [04/06/2025]. See the Terms and Conditions (https://onlinelibrary.wiley.com/terms-and-conditions) on Wiley Online Library for rules of use; OA articles are governed by the applicable Creative Commons License

different sources, CDs show high catalytic activity. The above discussion indicates that CDs have higher catalytic activity and a wider range of substrate concentrations and substrate types than natural enzymes, and the CDs can show catalytic activity without the addition of PBS, highlighting their potential as an efficient artificial enzyme catalyst. For industrial applications, the lifespan and cyclic stability of catalyst are key evaluation indicators as well. The reusability and recyclability of CDs were evaluated. As shown in Figure S10a (Supporting Information), the catalytic rate of CDs gradually decreased with the increase of substrate addition times, which may be related to the competition between the adsorption of CDs with substrates and the desorption of CDs with products. For the recyclability of CDs, we extracted the products and unfinished substrates by chloroform after the reaction, then lyophilized and recycled CDs. After 4 cycles, the catalytic activity of CDs is still greater than 80% (Figure S10b, Supporting Information). However, we found that the recovery rate of CDs after extraction and lyophilization was only ≈60%. Therefore, it is necessary to develop catalytic devices integrated with CDs to facilitate recycling.

Based on the high catalytic activity of CDs, they were adopted to construct a catalytic membrane to instantaneously hydrolyze esters during the process of passing through the membranes. An adhesive[40] was adopted for attaching CDs or lipase to filter paper. The SEM images (Figure S11, Supporting Information) and FTIR spectra (Figure S12, Supporting Information) of membranes were analyzed to demonstrate the integration of CDs on filter paper. Compared with the blank membrane, the surface of the CDs-integrated membrane was rough and uneven, and the characteristic signals from CDs/adhesive were observed. Then, the CDs-integrated membrane was used for the hydrolysis of *p*NPA. As shown in Videos S1–S5 (Supporting Information), we injected a *p*NPA water solution (2 mM, 6 mL) into the control filter (blank membrane, Video S1, Supporting Information) and filters containing either Lipase-integrated membranes (Video S5, Supporting Information) or CDs-integrated membranes (Videos S2–S4, Supporting Information) within 35 s. The corresponding snapshots are shown in Figure 3e, and Figure S13 (Supporting Information). Compared with the control (blank membranes), the filtrate from the CDs-integrated membrane (CDs×1) showed a yellow color due to the hydrolysate *p*NP, and their hydrolysate became more obvious with the increase of filtration membranes (CDs×2, CDs×4). However, the multilayer Lipase-integrated membranes (Lipase×4) could not achieve the hydrolysis of *p*NPA under the same catalytic conditions. We further calculated the single-pass conversion rates of CDs-integrated membranes with varying numbers of layers. As shown in Figure 3f, the conversion efficiency for a single-layer membrane is found to be 1.2%, and the conversion efficiency gradually increase with the increasing numbers of membrane layer. When passing through a five-layer CDs-integrated membranes, the conversion rate reached 24.5%. The results demonstrate that the CDs-integrated catalytic membrane can catalyze esters instantly, which has potential industrial application prospects.

We also evaluated and compared the stability of CDs and lipase under different conditions. Like other natural enzymes, lipase is sensitive to temperature. As displayed in **Figure 4**a, the catalytic activity of lipase for catalyzing the hydrolysis of 4-nitrophenyl acetate becomes inactive at high temperatures (>75 °C), and its optimum temperature (in PBS, pH = 7.00) is 37 °C. In contrast, the CDs show enhanced catalytic activity with increasing temperatures (5–75 °C). It is worth mentioning that the catalytic activity of CDs (60 μg mL^{-1}) not only can be significantly improved at high a temperature of 75 °C (126.4 mM min^{-1}), but also remains high (19.8 mM min^{-1}) at a low temperature of 5 °C. Furthermore, the heat pretreatment (50 °C for different times before use) of the CDs and lipase were carried out to investigate the temperature stability of them. After 12 h of heat pretreatment, the CDs still maintained catalytic activity, but lipase was deactivated after 1 h of heat pretreatment (Figure 4c). Regarding the tolerance to organic solvents and metallic salt solutions, the CDs display stable catalytic activity even in a high content of ethanol, while the lipase was inactivated when the ethanol content reached 40% (Figure 4b). Besides, the stability under different storage conditions was also analyzed (Figure 4d). At a storage temperature of 4 °C, the catalytic activity of lipase began to decrease gradually after 30 days, and completely deactivated after four months. However, the catalytic activity of CDs still keep for up to two years at 4 °C. At room temperature, the enzyme was completely deactivated for 30 days, but the CDs still had high catalytic activity after 200 days. Compared to natural enzymes, CDs have higher heat resistance, tolerance to organic solvents, and are easier to store. The good stability of CDs makes them more conducive to replacing natural enzymes for industrial applications.

2.4. The Catalytic Mechanism of the CDs as Hydrolase-Like Enzyme

An in-depth understanding of the catalytic mechanism of enzyme-like materials is beneficial for regulating their catalytic activity and expanding applications. Next, the catalytic mechanism of CDs as hydrolase-like artificial enzymes was investigated. In the previous section, we have discussed the interaction of one chain of CDs with *p*NPA and found that *p*NPA could be adsorbed by CDs via hydrogen bonds, making the ester bond of *p*NPA longer. To better simulate the catalytic environment, we also simulated the adsorption of *p*NPA by two chains under aqueous conditions. As shown in **Figure 5**a, compared with a single chain, two chains form more hydrogen bonds with *p*NPA and the system have lower energy, demonstrating that the CDs have strong adsorption under actual catalytic conditions. The adsorption site is located on the nitrogen atom of the cyclic dipeptide (unit of CDs). Moreover, similar to the theoretical calculation results for one chain, the ester bond of *p*NPA increases (from 1.379 to 1.398 Å) after it is adsorbed by CDs. The elongation of the ester bond makes *p*NPA easy to break and be hydrolyzed.

In order to further verify the adsorption sites of CDs, we measured the catalytic activity of CDs under different pH and metal ion conditions. As shown in Figure 5b, the CDs exhibit excellent catalytic activity in the pH range of 5 to 11, but their catalytic performance drops sharply at pH = 3. This is because the nitrogen on the cyclic dipeptide is protonated at pH = 3, affecting the hydrogen bonds between CDs and *p*NPA. In addition, when the CDs coordinate with metals, their catalytic activity for *p*NPA hydrolysis is also reduced. As displayed in Figure 5c, the

© 2024 Wiley-VCH GmbH

16163028, 2025, 17, Downloaded from https://advanced.onlinelibrary.wiley.com/doi/10.1002/adfm.202423470 by Soochow University, Wiley Online Library on [04/06/2025]. See the Terms and Conditions (https://onlinelibrary.wiley.com/terms-and-conditions) on Wiley Online Library for rules of use; OA articles are governed by the applicable Creative Commons License

16163028, 2025, 17, Downloaded from https://advanced.onlinelibrary.wiley.com/doi/10.1002/adfm.202424470 by Soochow University, Wiley Online Library on [04/06/2025]. See the Terms and Conditions (https://onlinelibrary.wiley.com/terms-and-conditions) on Wiley Online Library for rules of use; OA articles are governed by the applicable Creative Commons License

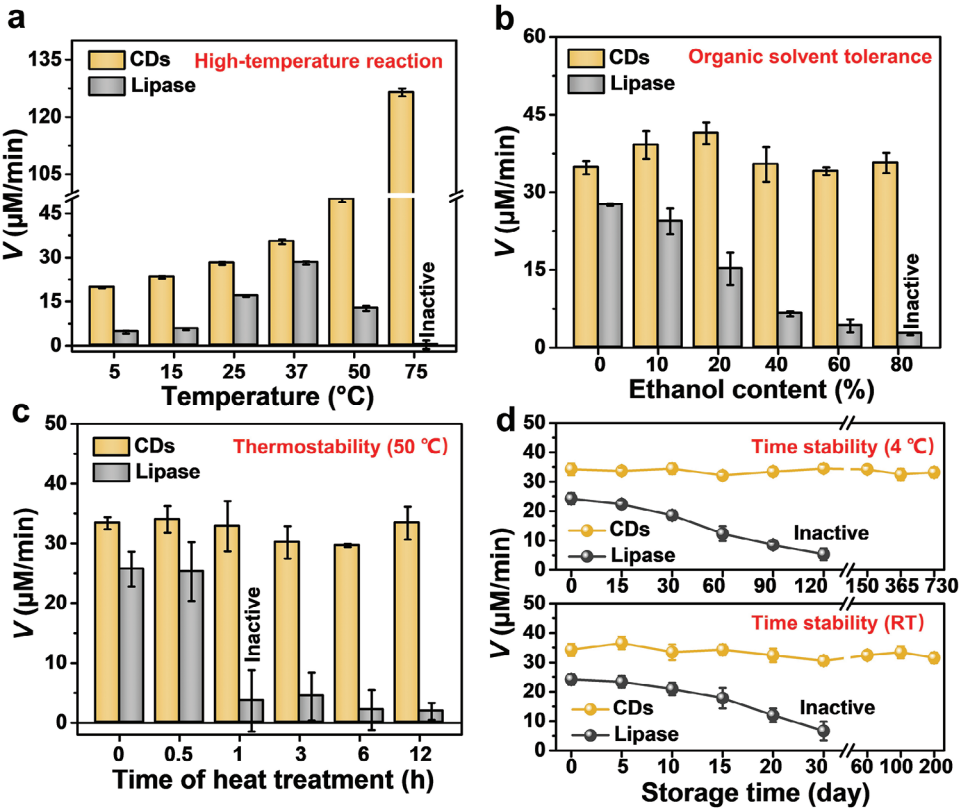


Figure 4. The catalytic activities of CDs (60 μg mL^{-1}, in H_2O, pH = 6.76) and lipase (60 μg mL^{-1}, in PBS, pH = 7.00) a) in different reaction temperatures (5–75 °C), b) in different ethanol contents (0–80%), c) under different pretreatment of heat (50 °C for 0, 0.5, 1, 3, 6, 12 h), and d) under different storage times (store conditions: 4 °C and room temperature). The concentration of pNPA is 2 mM.

ability of CDs to hydrolyze *p*NPA remains stable in the presence of Na^+, K^+, Mg^{2+}, and Ca^{2+}, but is inhibited by Mn^{2+}, Zn^{2+}, Co^{2+}, Cu^{2+} and Fe^{3+}. This is because Mn^{2+}, Zn^{2+}, Co^{2+}, Cu^{2+}, and Fe^{3+} have empty d orbitals that can coordinate with the nitrogen on the cyclic dipeptide, thus reducing the adsorption capacity of CDs to the substrates. The above experimental results further indicate that the adsorption site of CDs to *p*NPA is the nitrogen of the cyclic dipeptide of CDs.

Based on the above discussion, the catalytic mechanism of the CDs toward the hydrolysis of *p*NPA is illustrated in Figure 5d. A polymeric chain is used as the representative of CDs. The substrate *p*NPA is adsorbed onto the polycyclic dipeptide chain by hydrogen bonding, and the ester bond of *p*NPA is subsequently elongated. Then, CDs bind water molecule and stabilize and orient the hydroxide group for the nucleophilic attack on the *p*NPA adsorbed by CDs, thus breaking the ester bond and forming *p*NP.

3. Conclusion

In summary, we report that the cyclic dipeptide-based CDs possess superior hydrolase-like catalytic activity and kinetic characteristics of enzyme catalysis. Compared with lipase (Vm: 94 μM min^{-1}, in PBS), the CDs show higher catalytic activity (Vm: 268 μM min^{-1}, in H_2O) toward the hydrolysis of *p*NPA, and they exhiibit a wider range of substrate concentrations and substrate types. Besides, the CDs demonstrate higher heat resistance, tolerance to organic solvents, and are easier to store than lipase. Based on the high catalytic activity and stability of CDs, they were adopted for constructing an integrated catalytic membrane to directly hydrolyze esters during the process of passing through the CDs membranes instantly. The conversion rate reached 24.5% when passing through a five-layer CDs-integrated membranes. The highly efficient catalytic activity of CDs comes from their cyclic dipeptide structure, where the N in the cyclic dipeptide can effectively adsorb ester molecules, elongating the ester bond of substrates, and promoting hydrolysis. This work provides a deeper understanding of the enzyme-like catalytic activity of CDs, and provides a new path for obtaining efficient hydrolase-like materials.

4. Experimental Section

The synthesis of CDs: CDs were synthesized by electro-polymerization method using L type serine as raw material referred to previous work by the group.[26] Briefly, 3.00 g of L type serine and 1.20 g of NaOH were dissolved in 200 mL of ultrapure water. Two graphite rods as anode and cathode were inserted into the above solution with a constant voltage of 3.00 V, respectively. After 72 h, the solution was dialyzed against a 500–1000 Dalton cellulose dialysis bag to remove unreacted precursor and NaOH. Finally, the CDs were obtained.

The hydrolytic Activity Assay for CDs and Lipase: 4-Nitrophenyl acetate was chosen as a substrate and the absorbance of 405 nm (OD_{405}) for hydrolysate (4-Nitrophenol) was used to evaluate the hydrolytic activity assay

 © 2024 Wiley-VCH GmbH

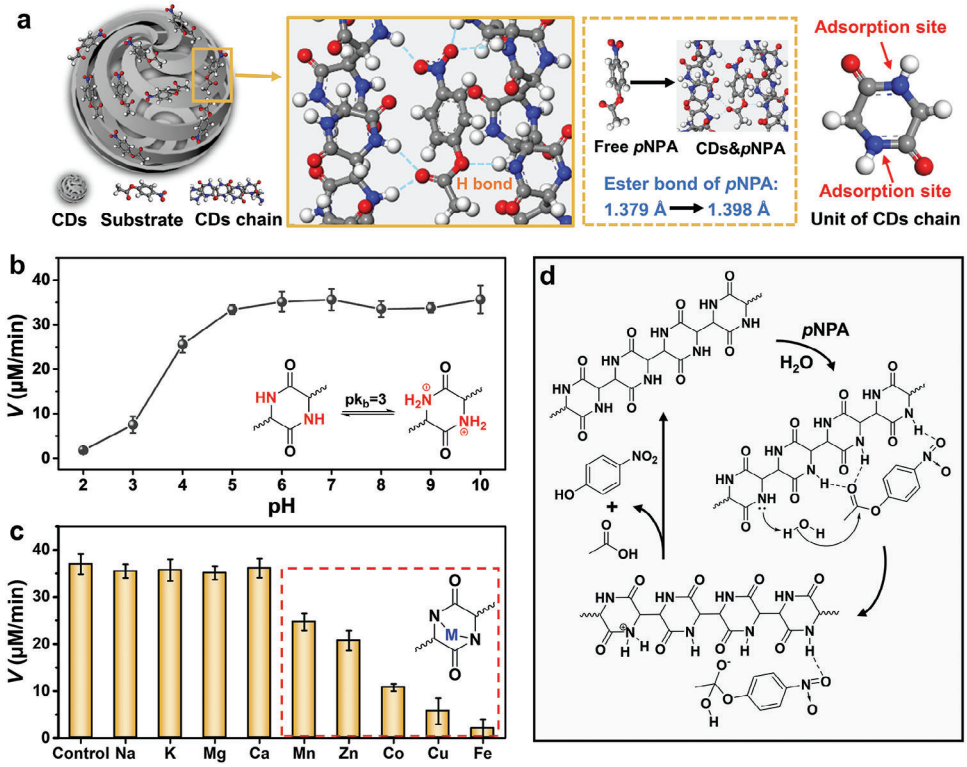


Figure 5. a) The adsorption and interaction of CDs with pNPA; The catalytic activities of CDs b) in different pH and c) in the exit of different metal ions (CDs/lipase: 60 μg mL^{-1}; *p*NPA is 2 mM; 37 °C); d) The catalytic mechanism of CDs toward the hydrolysis of *p*NPA.

of CDs and lipase. The reaction system contained: CDs or lipase (working concentration: 60 μg mL^{-1}) and 4-Nitrophenyl acetate (working concentration: 2 mM). For the lipase, the reaction system requires additional PBS (working concentration: 0.01 M, pH = 7.00). The mixtures were incubated at 37 °C for 20 min. Meanwhile, the 4-Nitrophenyl acetate in H_2O or PBS (0.01 M, pH = 7.00) was set as blank for eliminating the autohydrolysis of 4-Nitrophenyl acetate. The OD_{405} of the reaction systems were measured by a multifunctional microplate reader. The hydrolysate concentration could be converted by standard curve (4-Nitrophenol concentration vs OD_{405}), and finally, the hydrolytic activity ($\nu = C_{hydrolysate}/t$) could be obtained. It is worth noting that 4-Nitrophenol has different absorption coefficients in different environments, so the standard curve is determined in both lipase-PBS and CDs-H_2O systems. For other aromatic substrates (4-nitrophenyl formate, 4-nitrophenyl butyrate, 4-nitrophenyl pentanoate, 4-nitrophenyl phosphate ester), the hydrolytic activity of CDs was measured by similar methods. The experiment was performed three times for ensuring the accuracy of the results. The catalytic activity of chiral CDs and lipase was conducted in triplicate and the results were presented as mean ± standard deviation (SD).

The catalytic activity of CDs or lipase in the hydrolysis of olive oil was evaluated using acid-base titration. Under the catalysis of lipase, olive oil would produce fatty acids and glycerol, so the catalytic activity can be obtained by detecting the production rate of fatty acids. First, the olive oil and polyvinyl alcohol solution need to be ultrasonically prepared into an emulsion substrate by ultrasonic breaker. Then, CDs or lipase was added into emulsified olive oil, terminate the reaction with 95% ethanol. Finally, the amount of lactic acid produced was monitored by NaOH titration, and the catalytic activity of CDs or lipase could be calculated.

Kinetic Assay of Hydrolytic Activity for CDs and Lipase: The kinetic processes of CDs and lipase were measured by recording the OD_{405} of the hydrolysate of 4-Nitrophenyl acetate. The relationship between the enzymatic reaction velocity and substrate concentration was fitted to the Michaelis Menten equation, which was a classical model of the kinetics of the enzymatic reaction. Michaelis Menten equation was shown as follow:

$$V = \frac{[S] \times V_{max}}{[S] + K_m} \quad (1)$$

where V_{max} is the maximum reaction velocity, reflecting the catalytic activity, and K_m is the Michaelis constant, reflecting the affinity for substrates. V_{max} and K_m values could be plotted by Lineweaver Burk's double reciprocal plotting:

$$\frac{1}{V} = \frac{K_m}{V_{max}} \times \frac{1}{[S]} + \frac{1}{V_{max}} \quad (2)$$

By plotting the linear fit of the reciprocal of the reaction rate (1/V) against the reciprocal of the substrate concentration (1/[S]), the V_{max} and K_m values were calculated according to the slope and intercept.

Catalytic Stability Test for CDs and Lipase: The catalytic activities of CDs and lipase under heat pretreatment, in different reaction temperatures, pH values, ethanol contents, and metal ions were measured to compare the catalytic stability for CDs and lipase. For the heat pretreatment, CDs and lipase (60 μg mL^{-1}) were heated at 50 °C for 0.5, 1, 3, 6, 12 h, then their catalytic activities were evaluated. In addition, CDs or lipase (60 μg mL^{-1}), 4-Nitrophenyl acetate (2 mM) were mixed under different conditions, including temperature (5–75 °C), pH values (3 to 13), contents of organic solvent (ethanol, 0–80%) and metallic salt solutions (NaCl, KCl, $MgCl_2$, $FeCl_3$, $CoCl_2$, $ZnCl_2$, $CaCl_2$, $CuCl_2$, $MnCl_2$, $AlCl_3$; 100 μM). For the lipase, the reaction system requires additional PBS (pH = 7.00). The OD_{405} was recorded using a microplate reader after incubation of 20 min.

Catalytic Membrane Based on CDs and Lipase: An adhesive[40] was adopted for attaching CDs or lipase (1 mg) to filter paper (diameter 25 mm), and the obtained CDs-integrated membranes or Lipase-integrated membranes were placed into PP filter holders (where a blank

© 2024 Wiley-VCH GmbH

16163028, 2025, 17, Downloaded from https://advanced.onlinelibrary.wiley.com/doi/10.1002/adfm.202423470 by Soochow University, Wiley Online Library on [04/06/2025]. See the Terms and Conditions (https://onlinelibrary.wiley.com/terms-and-conditions) on Wiley Online Library for rules of use; OA articles are governed by the applicable Creative Commons License

filter paper membrane serves as a control), with three membranes placed in each filter holder. The above membranes were washed with deionized water, then *p*NPA water solution (2 mM, 6 mL) into a filter containing either a CDs-integrated membrane or Lipase-integrated membrane within 35 s, and the filtrates were collected. The number of membrane layers could be controlled by stacking filter holders.

Supporting Information

Supporting Information is available from the Wiley Online Library or from the author.

Acknowledgements

This work was supported by the National Key R&D Program of China (2024YFA1509303), Natural Science Foundation of Jiangsu Province (BE2022425, BK20230503), the National Natural Science Foundation of China (52302107, 52271223, 52272043), Project funded by the China Postdoctoral Science Foundation (2023M730044), State Key Laboratory of Catalysis (2024SKL-A-014), the Collaborative Innovation Center of Suzhou Nano Science & Technology, the 111 Project, and Suzhou Key Laboratory of Functional Nano & Soft Materials.

Conflict of Interest

The authors declare no conflict of interest.

Data Availability Statement

The data that support the findings of this study are available from the corresponding author upon reasonable request.

Keywords

carbon dots, catalytic kinetics, enzyme-like catalysis, hydrolase

Received: November 30, 2024
Published online: December 26, 2024

[1] D. Sutay Kocabaş, J. Lyne, Z. Ustunol, *Trends Food Sci. Technol.* **2022**, *119*, 467.
[2] O. L. Tavano, A. Berenguer-Murcia, F. Secundo, R. Fernandez-Lafuente, *Compreh. Rev. Food Sci. Food Saf.* **2018**, *17*, 412.
[3] Y. Cui, Y. Chen, J. Sun, T. Zhu, H. Pang, C. Li, W. C. Geng, B. Wu, *Nat. Commun.* **2024**, *15*, 1417.
[4] C. Guo, L. Q. Zhang, W. Jiang, *Chem* **2023**, *9*, 363.
[5] H. Lu, D. J. Diaz, N. J. Czarnecki, C. Zhu, W. Kim, R. Shroff, D. J. Acosta, B. R. Alexander, H. O. Cole, Y. Zhang, N. A. Lynd, A. D. Ellington, H. S. Alper, *Nature* **2022**, *604*, 662.
[6] S. P. Zhou, Y. P. Xue, Y. G. Zheng, *Biotechnol. Adv.* **2024**, *72*, 108352.
[7] M. D. Nothling, Z. Xiao, A. Bhaskaran, M. T. Blyth, C. W. Bennett, M. L. Coote, L. A. Connal, *ACS Catal.* **2018**, *9*, 168.
[8] T. Chen, Y. Lu, X. Xiong, M. Qiu, Y. Peng, Z. Xu, *Adv. Colloid Interface Sci.* **2024**, *323*, 103072.
[9] R. Zhang, X. Yan, K. Fan, *Acc. Mater. Res.* **2021**, *2*, 534.
[10] C. Zhang, X. Xue, Q. Luo, Y. Li, K. Yang, X. Zhuang, Y. Jiang, J. Zhang, J. Liu, G. Zou, X. J. Liang, *ACS Nano* **2014**, *8*, 11715.
[11] Y. M. Hur, K. I. Min, *Small Struct.* **2023**, *4*, 2200344.
[12] Y. Yuan, Y. Yang, M. Faheem, X. Zou, X. Ma, Z. Wang, Q. Meng, L. Wang, S. Zhao, G. Zhu, *Adv. Mater.* **2018**, *30*, 1800069.
[13] M. D. Arifuzzaman, I. Bose, F. Bahrami, Y. Zhao, *Chem Catalysis* **2022**, *2*, 2049.
[14] X. Li, M. Zangiabadi, Y. Zhao, *J. Am. Chem. Soc.* **2021**, *143*, 5172.
[15] M. Diez-Castellnou, F. Mancin, P. Scrimin, *J. Am. Chem. Soc.* **2014**, *136*, 1158.
[16] X. Huang, S. Zhang, Y. Tang, X. Zhang, Y. Bai, H. Pang, *Coord. Chem. Rev.* **2021**, *449*, 214216.
[17] X. Ma, L. Zhang, M. Xia, S. Li, X. Zhang, Y. Zhang, *ACS Appl. Mater. Interfaces* **2017**, *9*, 21089.
[18] R. Wang, K. Q. Lu, Z. R. Tang, Y. J. Xu, *J. Mater. Chem. A* **2017**, *5*, 3717.
[19] Y. Zhai, B. Zhang, R. Shi, S. Zhang, Y. Liu, B. Wang, K. Zhang, G. I. N. Waterhouse, T. Zhang, S. Lu, *Adv. Energy Mater.* **2021**, *12*, 2103426.
[20] M. Zhang, Y. Ma, H. Wang, B. Wang, Y. Zhou, Y. Liu, M. Shao, H. Huang, F. Lu, Z. Kang, *ACS Appl. Mater. Interfaces* **2021**, *13*, 5877.
[21] E. Ozyilmaz, O. Caglar, I. Sargin, G. Arslan, *Mater. Today Commun.* **2022**, *30*, 103066.
[22] W. Yang, T. Leng, W. Miao, X. Cao, H. Chen, F. Xu, Y. Fang, *Angew. Chem., Int. Ed.* **2024**, *63*, 202403581.
[23] Y. Ma, M. Zhang, J. Wu, Y. Zhao, X. Du, H. Huang, Y. Zhou, Y. Liu, Z. Kang, *Small* **2023**, *19*, 2300883.
[24] B. Kong, T. Yang, F. Cheng, Y. Qian, C. Li, L. Zhan, Y. Li, H. Zou, C. Huang, *J. Colloid Interface Sci.* **2022**, *611*, 545.
[25] X. Li, S. Ding, Z. Lyu, P. Tieu, M. Wang, Z. Feng, X. Pan, Y. Zhou, X. Niu, D. Du, W. Zhu, Y. Lin, *Small* **2022**, *18*, 2203001.
[26] M. Zhang, W. Zhang, X. Fan, Y. Ma, H. Huang, X. Wang, Y. Liu, H. Lin, Y. Li, H. Tian, M. Shao, Z. Kang, *Nano Lett.* **2022**, *22*, 7203.
[27] W. Gao, J. He, L. Chen, X. Meng, Y. Ma, L. Cheng, K. Tu, X. Gao, C. Liu, M. Zhang, K. Fan, D. W. Pang, X. Yan, *Nat. Commun.* **2023**, *14*, 160.
[28] J. Du, S. Qi, J. Chen, Y. Yang, T. Fan, P. Zhang, S. Zhuo, C. Zhu, *RSC Adv.* **2020**, *10*, 41551.
[29] Y. Wang, T. Pan, J. Li, L. Zou, X. Wei, Q. Zhang, T. Wei, L. Xu, R. V. Ulijn, C. Zhang, *ACS Appl. Mater. Interfaces* **2024**, *16*, 22369.
[30] J. Han, Q. Zou, W. Su, X. Yan, *Chem. Eng. J.* **2020**, *394*, 124987.
[31] J. Liu, S. Sun, R. Lv, S. Lin, Y. A. Golubev, K. Wang, R. Cao, Y. Zeng, *Sep. Purif. Technol.* **2025**, *354*, 128979.
[32] F. Li, Y. Li, X. Yang, X. Han, Y. Jiao, T. Wei, D. Yang, H. Xu, G. Nie, *Angew. Chem., Int. Ed.* **2018**, *57*, 2377.
[33] Y. Ru, L. Sui, H. Song, X. Liu, Z. Tang, S. Q. Zang, B. Yang, S. Lu, *Angew. Chem., Int. Ed.* **2021**, *60*, 14091.
[34] C. Xia, Y. Qiu, Y. Xia, P. Zhu, G. King, X. Zhang, Z. Wu, J. Y. Kim, D. A. Cullen, D. Zheng, P. Li, M. Shakouri, E. Heredia, P. Cui, H. N. Alshareef, Y. Hu, H. Wang, *Nat. Chem.* **2021**, *13*, 887.
[35] E. Shuang, C. He, J. H. Wang, Q. Mao, X. Chen, *ACS Nano* **2021**, *15*, 14465.
[36] M. Zhang, Y. Zhang, X. Du, Y. Ma, H. Huang, F. Liao, X. Fan, J. Wang, H. Lin, M. Shao, Y. Liu, Y. Li, Z. Kang, *ACS Appl. Mater. Interfaces* **2024**, *16*, 19379.
[37] Q. Wu, J. Cao, X. Wang, Y. Liu, Y. Zhao, H. Wang, Y. Liu, H. Huang, F. Liao, M. Shao, Z. Kang, *Nat. Commun.* **2021**, *12*, 483.
[38] L. Đorđević, F. Arcudi, A. D'Urso, M. Cacioppo, N. Micali, T. Bürgi, R. Purrello, M. Prato, *Nat. Commun.* **2018**, *9*, 3442.
[39] H. Li, C. Sun, M. Zhang, W. Yan, Z. Kang, *Adv. Funct. Mater.* **2024**, *34*, 2405669.
[40] C. R. Westerman, B. C. McGill, J. J. Wilker, *Nature* **2023**, *621*, 306.

© 2024 Wiley-VCH GmbH

16163028, 2025, 17, Downloaded from https://advanced.onlinelibrary.wiley.com/doi/10.1002/adfm.202423470 by Soochow University, Wiley Online Library on [04/06/2025]. See the Terms and Conditions (https://onlinelibrary.wiley.com/terms-and-conditions) on Wiley Online Library for rules of use; OA articles are governed by the applicable Creative Commons License

Vol. 35 • No. 17 • April 25 • 2025

www.afm-journal.de

ADVANCED FUNCTIONAL MATERIALS



WILEY VCH

创新创业学分认定诚信声明

本人郑重声明：所提交的用以申请创新创业学分认定的内容(包括但不限于学科竞赛获奖、学术论文、科研项目成果、专利创造成果、文学艺术类成果以及创业实践类成果等)均为本人在校期间原创取得，不存在任何侵权、造假等违规行为。

本人完全意识到本声明的法律后果由本人承担。本人所提交的内容如涉嫌违规违法，本人愿意承担相应后果。

申请人签名：吴泽雨

指导（证明）老师签名：

2024年6月5日

专家鉴定意见

本人作为纳米材料与技术领域的专业研究人员，经审核确认，论文（标题为 Carbon Dots with Polycyclic Dipeptide Structure Surpass Natural Hydrolase Performance）聚焦于具有多环二肽结构的碳点优于天然水解酶性能，与纳米材料与技术专业核心方向高度契合。

本人作为指导老师，对成果的原创性、真实性及学术规范性予以确认。

推荐人签名：

2025 年 6 月 9 号